Intramolecular vibrational relaxation of a polyatomic in the solid state. II. HC1 4N and HC1 5N in Ar, Kr, and Xe

Alison D. Abbate and C. Bradley Moore

Citation: The Journal of Chemical Physics **83**, 975 (1985); doi: 10.1063/1.449425
View online: http://dx.doi.org/10.1063/1.449425
View Table of Contents: http://scitation.aip.org/content/aip/journal/jcp/83/3?ver=pdfcov
Published by the AIP Publishing

Intramolecular vibrational relaxation of a polyatomic in the solid state. II. $HC^{14}N$ and $HC^{15}N$ in Ar, Kr, and Xe

Alison D. Abbate[a] and C. Bradley Moore
Department of Chemistry, University of California, Berkeley, California 94720

(Received 16 August 1984; accepted 24 April 1985)

The vibrational relaxation of $HC^{14}N$ and $HC^{15}N$ isolated in Ar, Kr, and Xe matrices was studied by laser-excited vibrational fluorescence. Complete sets of rate constants for the unimolecular relaxation of ν_3 excitation through the ν_1 and ν_2 manifolds were obtained for HCN/Xe. At low temperatures the $(1,0^0,0)$ level is a metastable trap and at increased temperatures detrapping shifts the relaxation route from the ν_1 to the ν_2 manifold. Dipole–dipole hopping of ν_3 and ν_2 quanta was observed and treated quantitatively with Förster theory. The temperature dependence of rates indicates that the vibrational energy is transferred to a local guest mode. The increase in rate, $k_{Xe} < k_{Kr} < k_{Ar}$, with steepness of repulsive potential and with vibrational frequency in the matrix shows that relaxation is caused by a repulsive interaction between guest and matrix. Gas phase theory is adapted to model hard "collisions" with the matrix cage; it indicates that translation rather than rotation is the accepting mode. The success of this model in treating the dependence of rate on vibrational energy and quantum number change suggests that it will be useful for predicting relaxation mechanisms and rates in other systems.

I. INTRODUCTION

The preceding study of DCN in Xe[1] yielded detailed information on the intramolecular vibrational relaxation of a matrix isolated polyatomic molecule. After excitation of the C–D stretch, ν_3, the rise and fall of fluorescence from lower levels in both the CN stretch, ν_1, and the bend, ν_2, manifolds was measured and these time dependent populations were fit with a comprehensive kinetic scheme. The sequential loss of bending quanta was found to be consistent with the simplest predictions for relaxation of a harmonic oscillator. Such has previously been found for the C–F stretch in CH_3F.[2,3] For transfers from one vibrational mode to another no simple correlation of rate constant with net energy lost from vibration was apparent. The present study of the relaxation of matrix isolated HCN builds on the DCN results. The isotopic shifts in energy levels, Fig. 1, introduce some new nonradiative transitions between the ν_1 and ν_2 manifolds and provide different energy gaps for some transitions which were already measured for DCN. In addition to finding the rate constants for relaxation at 9 K, this HCN investigation looks at several other factors in the relaxation. The previous spectroscopic study[4] showed that there are two trapping sites for HCN/Xe. The effect of site-selective excitation on subsequent relaxation is studied. The concentration of guest molecules is varied to distinguish between inter- and intramolecular energy transfer.

The kinetic scheme for relaxation of HCN is complicated by the near resonance of the C–N stretch with three quanta of the bend, Fig. 1. As a consequence it is possible to study the behavior of the ν_1 level as a metastable trap. The acceleration of relaxation by thermal activation from ν_1 to $3\nu_2$ as the temperature is increased results in an "anomalously" large temperature dependence of the ν_1 relaxation rate. The change in rates with rare gas host is correlated to the matrix shift in vibrational frequency and suggests a dynamical mechanism for the relaxation event.

Ten different energy transfer rate constants are now known for the various isotopic hydrogen cyanide molecules isolated in Xe. The simplest theory[5] for vibrational energy transfers in gas phase collisions is adapted to model "collisions" with the repulsive wall of the matrix cage. This provides a simple model for the combined effects of energy loss and quantum number change on the rates of transfer from one vibration to another. The fit of the rate constants allows a choice between rotation and translation as the local mode which accepts the vibrational energy. The model should be generally useful for making rough estimates of relative relaxation rates.

HCN exhibits inter- as well as intramolecular energy transfer even in highly dilute matrices ($M/A > 5000$). Monitoring the concentration dependence of the population of the $\nu_1 + \nu_2$ level allows a direct measurement of the resonant dipole–dipole hopping rate of a ν_2 quantum to a ground state molecule. Intermolecular energy transfer has been observed experimentally[3,6–11] and treated theoretically[12–16] by numerous investigators. The theoretical papers explicitly treat dipole–dipole (Förster) transfer, for either resonant exchange[12] or for the more complicated case of phonon-assisted transfer.[13]

Intermolecular vibrational energy transfer was first observed by Dubost and Charneau[6] for CO/Ne, Ar and later by Apkarian and Weitz[3] for CH_3F/Kr, Xe where emission from overtones and different isotopic species followed excitation of a fundamental stretch. In this way laser action has been observed from $v = 2 \rightarrow v = 1$ of CN^-.[11] Dubost and Charneau[6] were unable to fit the rise in ^{13}CO population by calculating the hopping rate from ^{12}CO. Manz[14] successfully modeled the time evolution of their ^{12}CO vibrational levels by deriving hopping rates to higher vibrational levels as multiples of $k(1,1 \rightarrow 0,2)$, the rate at which two molecules in $v = 1$ yield one in $v = 2$. This rate constant was adjusted to bring

[a] Present address: Solar Energy Research Institute, 1617 Cole Boulevard, Golden, CO 80401.

 0021-9606/85/150975-18$02.10

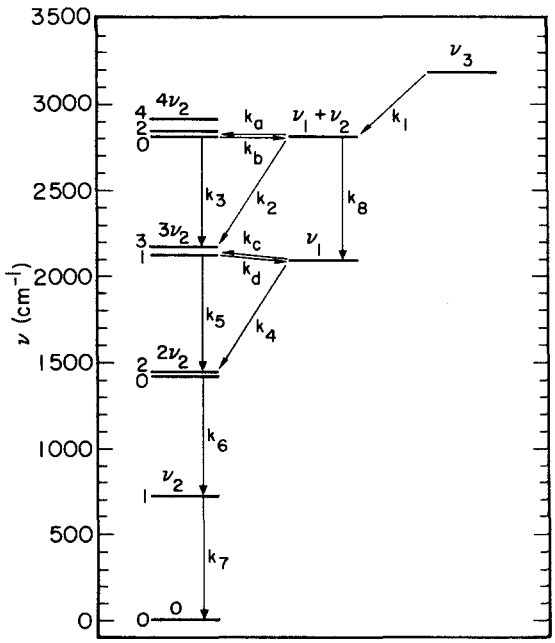

FIG. 1. Energy level diagram for HCN/Xe, site 1, 9 K, showing kinetic scheme for relaxation. For the ν_2 levels the l quantum number is labeled.

agreement of theoretical and experimental results rather than calculated directly from a model of dipole–dipole transfer. Hopping from an excited molecule to a different guest species was observed for ND→CO in Ar[8] and for C_2^- →C_2H_2 in Ar.[9] Goodman and Brus[8] were able to fit the CO rise to the nonexponential form expected for dipole–dipole transfer by varying the magnitude of the energy transfer rate constant. However, the C_2^- decay could not be fit using the analogous equation for the appropriate quadrupole interactions.[9]

The above demonstrations of intermolecular vibrational energy transfer are all nonresonant processes and therefore difficult to model directly from dipole–dipole transfer theory. Resonant hops of $v = 1$ excitations do not change the excited state population and thus have not been experimentally observed. The hopping of a ν_2 quantum from the HCN combination level $\nu_1 + \nu_2$ results in a net change in excited level populations and this offers a novel opportunity to observe resonant energy transfer directly and to compare it to Förster's model. This is then the first direct test of Förster theory without adjustable parameters against data for vibrational energy transfer in a solid.

II. EXPERIMENTAL

The preparation and characterization of the HCN matrices is described in the preceding spectroscopic study.[4] The vibrational energy levels of HCN/Xe are shown in Fig. 1. The laser-induced fluorescence technique is described in the kinetic study of DCN/Xe.[1] Fluorescence from different vibrational levels was separated by either a 3–6 μm circular variable filter (CVF) or a pair of CVF's covering the ranges 3.8–7.6 and 7.1–14.1 μm. The FWHM resolution of this pair of CVF's in wavelength regions of interest in the experiments was 1.04% at 14 μm, 1.05% at 7 μm, and 1.09% at 5 μm.

TABLE I. Deposition and fluorescence conditions for matrices, in chronological order.

Matrix	Guest	Host	M/A	mmol[a]	$T_{dep.}$	T_n^b	CVF (μm)
2	HCN	Xe	1 070	3.9	25[c]	9.0,20.0,32.5	
3	HCN	Xe	4 950	15.5	25[c]	9.0,20.1,30.6	
5	HCN	Ar	5 020	30.7	9[d]	9.0,19.8	
11	HCN	Xe	5 560	14.8	9	9.0	3–6
14	HCN	Ar	5 050	19.4	9	9.0	3–6
17	HCN	Xe	19 060	21.2	9	9.0,16.9	3–6
18	HCN	Xe	900	4.2	9	9.0	3–6
22	HCN	Xe	5 690	17.6	9	9.0,21.4,30.1	4–14
23	HCN	Xe	5 140	15.9	9	15.0,11.9,9.0	4–14
24	DCN[e]	Xe	4 890	14.8	9	9.0,18.1	4–14
25	HCN	Xe	410	17.6	9	9.0	4–14
28	HCN	Xe	10 310	12.0	9	9.0	4–14
29	$HC^{15}N$	Xe	7 020	16.2	9	9.0,15.2	4–14
30	$HC^{15}N$	Ar	7 260	19.0	9	9.0	4–14
32	$HC^{15}N$	Xe	7 210	27.0	20	9.0,15.2,20.8, 25.3,12.2,18.1, 30.0	4–14
34	$HC^{15}N$	Kr	5 820	24.0	9	9.0,18.2,25.0	4–14
38	DCN[f]	Xe	6 270	21.9	9	9.0,15.5,21.3, 27.6	4–14
40	$HC^{15}N$	Xe	8 470	27.2	9	9.0	4–14

[a] Total mmol of gas mixture deposited determined by pressure change.
[b] Temperatures listed in the order they were measured.
[c] Annealed to 40 K.
[d] Annealed to 20 K.
[e] 87% deuterated.
[f] 92% deuterated.

III. RESULTS

A. Systems studied

The composition and deposition conditions for the matrices studied in fluorescence are listed in Table I. This table includes the DCN matrices from Ref. 1 but not those matrices which were used only for spectroscopy.

Excitation of the C–H stretch, ν_3, of HCN in rare gas matrices produced observable fluorescence from many lower energy levels. Since the rates were slowest in Xe, it was used for most of the experiments. Fluorescence from the difference frequency transition $(0,0^0,1)$–$(0,1^1,0)$ allowed ν_3 to be observed without interference from scattered laser light. The $(1,0^0,0)$ level could be seen with the transitions $(1,0^0,0)$–$(0,0^0,0)$ or $(1,0^0,0)$–$(0,1^1,0)$ and $(1,1^1,0)$ could be seen with the analogous transitions. The $(1,1^1,0)$ level could also be seen by emission of one ν_2 quantum or by emission to the ground state. The ν_2 levels could be observed by $\Delta v_2 = 1$ or 2 transitions. Some transitions were too close in frequency to be completely resolved. Table II shows the quantum states and frequencies of the observed transitions and lists any other levels whose fluorescence could not be eliminated. The following convention is used: a hyphen between levels indicates fluorescence, an arrow indicates a nonradiative transition.

Matrix-to-matrix reproducibility was excellent. The fluorescence from each matrix was compared to previous ones by simultaneously graphing traces for comparable M/A at the same temperature and CVF setting. They were generally perfectly superimposable, even for levels with S/N > 100 where very small differences would have been noted. The only exception was the fluorescence with contributions from both $(1,1^1,0)$–$(1,0^0,0)$ and $(0,1^1,0)$–$(0,0^0,0)$. These traces have a fast component from $(1,1^1,0)$ and a much slower one from $(0,1^1,0)$. The relative amplitudes of these contributions varied (by less than 50%) between matrices, presumably due to changes in the amount of self-absorption of $(0,1^1,0)$ as the concentration varied in the range of $M/A = 6000$ (see Table I) and the angle at which the laser hit the matrix varied from 45°. In addition, the $(1,1^1,0)$ decay and the $(0,1^1,0)$ rise have contributions from intermolecular energy transfers which are expected to be sensitive to matrix preparation. The decay rates were identical in spite of amplitude differences.

TABLE II. Transitions observed in fluorescence of HCN/Xe.

Transition	$\nu(\text{cm}^{-1})$[a] HC^{14}N	HC^{15}N	Overlapping transitions
$(0,0^0,1)$–$(0,1^1,0)$	2563.3	2562.8	
$(1,1^1,0)$–$(0,0^0,0)$	2803.4	2770.1	
$(1,1^1,0)$–$(1,0^0,0)$	713.9	712.9	$(0,1^1,0)$–$(0,0^0,0)$ $(0,2^0,0)$–$(0,1^1,0)$ $(0,2^2,0)$–$(0,1^1,0)$
$(1,1^1,0)$–$(0,1^1,0)$	2086.7	2054.4	$(1,0^0,0)$–$(0,0^0,0)$
$(1,1^1,0)$–$(0,2^0,0)$	1385.5	1354.1	$(1,0^0,0)$–$(0,1^1,0)$
$(1,1^1,0)$–$(0,2^2,0)$	1364.4	1333.2	$(1,0^0,0)$–$(0,1^1,0)$
$(1,0^0,0)$–$(0,0^0,0)$	2089.5	2057.2	$(1,1^1,0)$–$(0,1^1,0)$
$(1,0^0,0)$–$(0,1^1,0)$	1372.8	1341.5	$(1,1^1,0)$–$(0,2^0,0)$ $(1,1^1,0)$–$(0,2^2,0)$
$(0,4^0,0)$–$(0,2^0,0)$] $(0,4^2,0)$–$(0,2^2,0)$]	1398.1	1396.3	$(0,3^1,0)$–$(0,1^1,0)$ $(0,2^0,0)$–$(0,0^0,0)$
$(0,3^1,0)$–$(0,1^1,0)$	1408.0	1406.1	$(0,4^0,0)$–$(0,2^0,0)$ $(0,4^2,0)$–$(0,2^2,0)$ $(0,2^0,0)$–$(0,0^0,0)$
$(0,2^0,0)$–$(0,0^0,0)$	1417.9	1416.0	$(0,3^1,0)$–$(0,1^1,0)$ $(0,4^0,0)$–$(0,2^0,0)$ $(0,4^2,0)$–$(0,2^2,0)$
$(0,1^1,0)$–$(0,0^0,0)$[b]	716.7	715.7	$(1,1^1,0)$–$(1,0^0,0)$ $(0,2^2,0)$–$(0,1^1,0)$

[a] Transition frequencies are given for site 1.

[b] The $\Delta v_2 = 1$ transitions are too close to separate because of the various l levels. The $(0,1^1,0)$ level can be partially separated in HC^{15}N at 9 K because $(0,3^1,0)$ and $(0,4^0,0)$ have no population.

B. Multiple sites

The infrared spectra[4] show that there are two trapping sites for HCN in Xe, one of which (site 2) splits the ν_2 degeneracy. To see if a kinetic difference would correspond to this spectroscopic difference, the two ν_3 peaks were excited separately. They were excited on the outer edge of the bands because the laser linewidth is 2 cm^{-1} FWHM and the lines are separated by 4 cm^{-1}. Fluorescence from ν_3 (Fig. 2) shows that the higher energy band (site 1) relaxes more slowly. Fluorescence from lower levels showed no change with excitation frequency. Since the fluorescence is not affected, the center of the stronger band (site 2) was excited in these experiments unless otherwise specified. The frequency was 3276.2 cm^{-1} for HC^{14}N/Xe and 3274.9 cm^{-1} for HC^{15}N/Xe.

C. Concentration effect

Fluorescence from ν_3 at $M/A = 19\,060$ and 900 is shown for comparison with single exponential fits in Fig. 2. The decay cannot be described with a single exponential even at high dilution. While increasing the concentration does not markedly increase the rate, the decay does become less exponential.

The $(1,1^1,0)$ level has the largest increase in decay rate with concentration. It also becomes increasingly nonexponential at high concentrations. Figure 3 shows the decay rates of $(0,0^0,1)$ and $(1,1^1,0)$ as a function of dilution. The decays are approximated with a single exponential and the "error" bars correspond to fitting the fast and slow portions of the decay. These decays are nonexponential and cannot be fit meaningfully with either single or double exponential functions. They have been approximated as single exponential decays, i.e., slopes of the semilog plot at various points in the decay, in order to show the magnitude of the decay rates and the deviation from single exponential decay. Even with the high S/N for ν_3 fluorescence, amplitude and rate parameters for bi- or multiexponential fits cannot be reliably determined

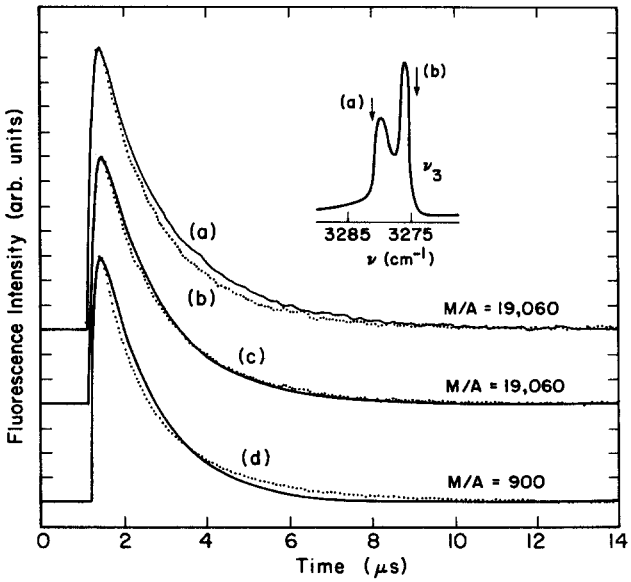

FIG. 2. Effect of excitation frequency and concentration on $(0,0^0,1)$–$(0,1^1,0)$ fluorescence of HCN/Xe. For matrix 17, $M/A = 19\,060$, $T = 9$ K, molecules in the two trapping sites were excited at the frequencies indicated by the arrows: (a) 3281.1 cm^{-1} and (b) 3273.8 cm^{-1}. Exponential fits to this data give decay rates of (a) 6.0×10^5 s^{-1} and (b) 6.4×10^5 s^{-1}. The concentration dependence of $(0,0^0,1)$ fluorescence with excitation at 3276.2 cm^{-1} is shown in (c), matrix 17, $M/A = 19\,060$ with a fit which rises with detector response, $k_{det} = 1.1\times10^7$ s^{-1}, and falls with $k = 6.3\times10^5$ s^{-1}, and in (d), matrix 18, $M/A = 900$, with a fit that falls with $k = 7.4\times10^5$ s^{-1}. As the concentration is increased the decay deviates more from a single exponential.

when the logarithmic time derivative varies by only 10% to 30% throughout a decay. The matrices used to determine the unimolecular relaxation rates have $M/A > 5000$. Figure 3 shows that, except for the $(1,1^1,0)$ decay, this can be considered infinite dilution.

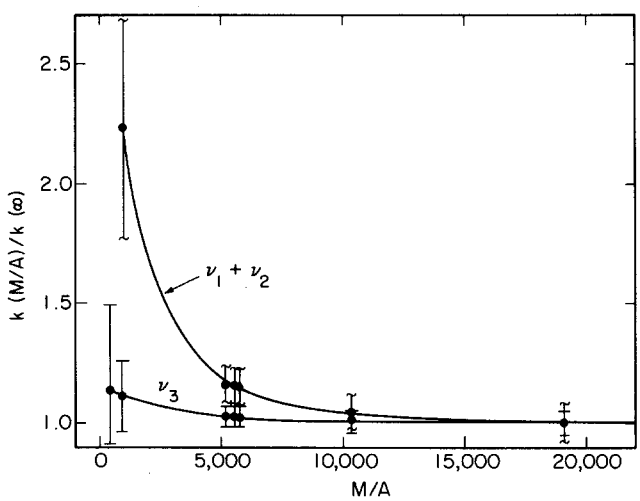

FIG. 3. Increase in $(1,1^1,0)$ and $(0,0^0,1)$ decay rates with increase in concentration of HCN/Xe at 9 K. These k's correspond to λ_2 and λ_1, respectively, in Table V. Rates are normalized to the rates at $M/A = 19\,060$: $k_{001} = (6.3\pm0.3)\times10^5$ s^{-1} and $k_{110} = (1.3\pm0.1)\times10^5$ s^{-1}. "Error bars" are fits to fast and slow portions of multiple exponential decays. They get wider with increased concentration.

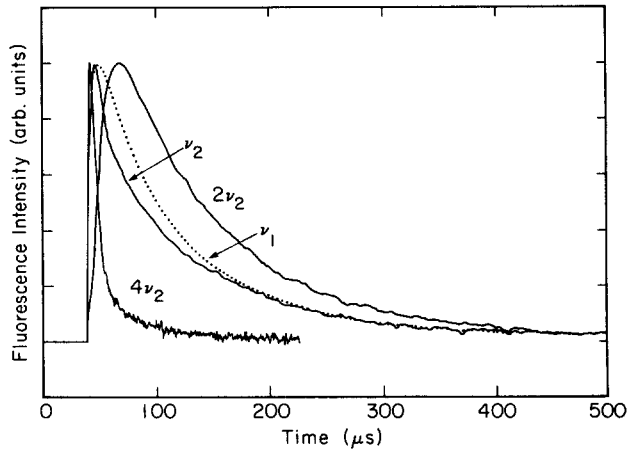

FIG. 4. Fluorescence from $4\nu_2$, $2\nu_2$, ν_2, and ν_1 of HCN/Xe, matrix 22, $M/A = 5690$, 9 K. These levels dominate the fluorescence with the CVF at: 1398 cm^{-1} for $(0,4^0,0)$–$(0,2^0,0)$, 1424 cm^{-1} for $(0,2^0,0)$–$(0,0^0,0)$, 717 cm^{-1} for $(0,1^1,0)$–$(0,0^0,0)$, and 2084 cm^{-1} for $(1,0^0,0)$–$(0,0^0,0)$. The fast component in the ν_2 trace is $(1,1^1,0)$–$(1,0^0,0)$ fluorescence which is not sufficiently to the red to be filtered out completely by the CVF (see Table II). Because of interference from other transitions (Table II), the frequency of maximum filter transmission which best isolates a given transition is not always the same as the transition frequency. For a harmonic oscillator a factor of 2 increase in rate is expected for $4\nu_2$ compared to $2\nu_2$ and for $2\nu_2$ compared to ν_2.

D. Qualitative behavior of fluorescence decay rates

Fluorescence from the $4\nu_2$ and $2\nu_2$ levels of HCN/Xe is shown in Fig. 4. Reference 1 showed that the relaxation rates for $\Delta v_2 = -1$ in the ν_2 manifold of DCN/Xe are consistent with the harmonic oscillator relation: $k_{v,v-1} = vk_{1,0}$. If HCN/Xe follows this rule, there should be a factor of 2 difference in the decay rates of $4\nu_2$ and $2\nu_2$. However, there is more than an order of magnitude difference. Similarly, the decay rate of $2\nu_2$ should be twice that of ν_2. Figure 4 shows that they differ by less than a factor of 2. The decay rate of ν_1 fluorescence is unexpectedly similar to that of ν_2 and $2\nu_2$.

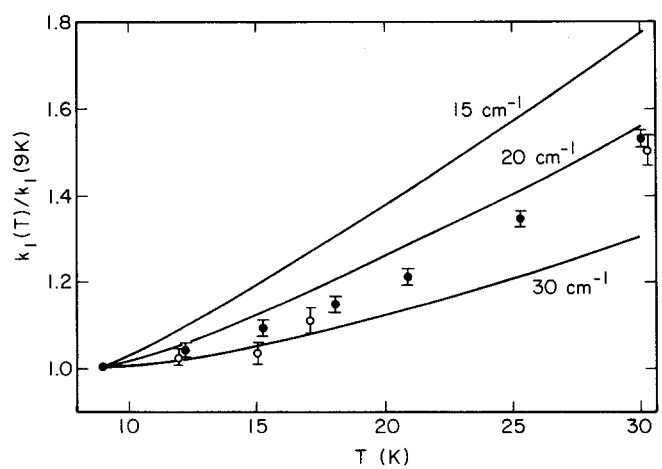

FIG. 5. Decay of $(0,0^0,1)$, k_1, in $HC^{15}N$/Xe, matrix 32 (filled circles), and $HC^{14}N$/Xe, matrices 17, 22, and 23 (open circles), as a function of temperature. The data are normalized to the 9 K rate constants, $k_1 = 4.7\times10^5$ and 6.3×10^5 s^{-1} for the ^{15}N and ^{14}N isotopes, respectively. The solid lines show the temperature dependence expected for a process requiring excitation of a single phonon to conserve energy in the relaxation.

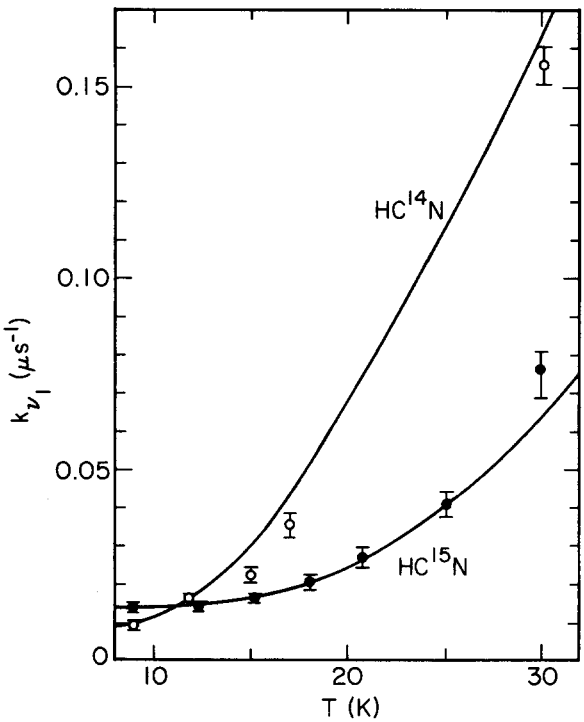

FIG. 6. Temperature dependence of $(1,0^0,0)$ decay in HC^{15}N/Xe, matrix 32, and HC^{14}N/Xe, matrices 17, 22, and 23. Fluorescence was observed through the $(1,0^0,0)$–$(0,1^1,0)$ transition with the CVF at 1340 cm^{-1} for HC^{15}N and 1380 cm^{-1} for HC^{14}N. The solid lines show the temperature dependence expected if the increase in rate is dominated by a Boltzmann shift in equilibrium k_a vs k_b and k_c vs k_d.

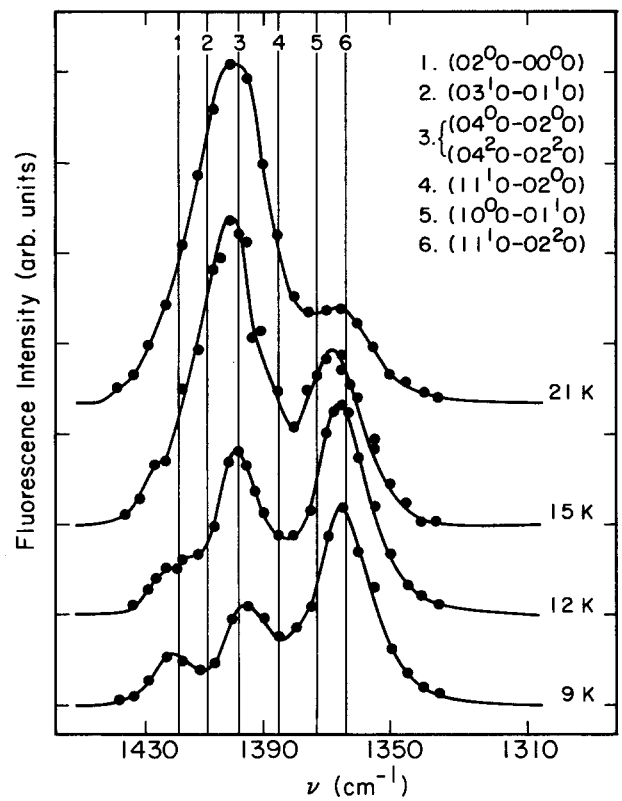

FIG. 7. Emission spectra for various temperatures for HCN/Xe. The spectra have been vertically displaced for clarity. Matrix 22, $M/A = 5690$, gave $T = 9$ and 21 K data. Matrix 23, $M/A = 5140$, gave $T = 9$, 12, and 15 K data. The signal is normalized to the 9 K data for each matrix. Peak fluorescence intensity, normalized for laser energy, is plotted as a function of CVF transmission frequency. The vertical lines show the frequencies of HCN/Xe fluorescence transitions in this region.

The rate of ν_3 relaxation shows little change with temperature (Fig. 5). This temperature dependence is comparable to that for the ν_2 manifold of DCN/Xe. It was demonstrated for DCN that this is consistent with a model[17] in which the vibrational energy is transferred to local guest translation or rotation with the emission of one phonon to match the energy levels. In contrast, the ν_1 decay rate for HC^{14}N increases by a factor of 15 between 9 and 30 K (Fig. 6). This is an unusually large temperature dependence for the vibrational relaxation of a matrix isolated molecule.

Emission spectra (Fig. 7) show the relative intensity of fluorescence from various levels. The maximum amplitude of each fluorescence trace is plotted vs the CVF transmission frequency. The fluorescence intensity is proportional to the population and to the Einstein A value of the transition. These spectra have not been normalized by dividing by A because several levels overlap at each frequency. At 9 K most of the fluorescence comes from the $(1,1^1,0)$ and $(1,0^0,0)$ levels. As the temperature is increased, the $(0,4^0,0)$, $(0,3^1,0)$, and $(0,2^0,0)$ emission increases. Figure 8 shows similar emission spectra for HC^{15}N/Xe at several temperatures.

E. Host effect

There is a large increase in relaxation rates as the matrix host is changed from Xe to Kr to Ar. With this change in host the ν_3 relaxation rate of HC^{15}N increases by a factor of 3.4 and the ν_1 relaxation rate increases by a factor of 41. Figures 9 and 10 show these rates graphed vs the matrix shifts.

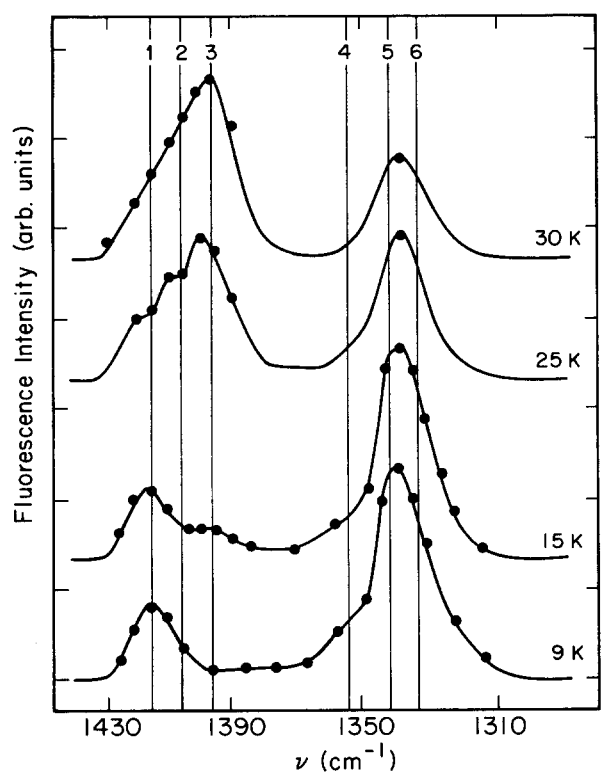

FIG. 8. Emission spectra for HC^{15}N/Xe, matrix 32, $M/A = 7210$, at various temperatures. Vertical lines show frequencies for transitions as labeled in Fig. 7.

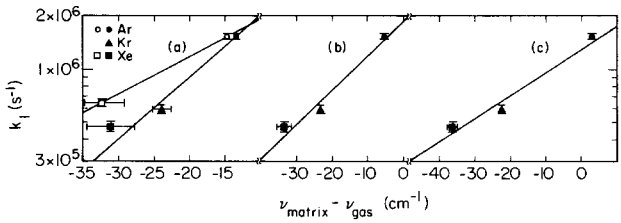

FIG. 9. Rate of ν_3 decay for different hosts correlated with the matrix shift in the frequency of (a) the $(0,0^0,1) \rightarrow (1,1^1,0)$ nonradiative transition, (b) the $(0,0^0,1)$ level, and (c) the sum of the $(0,0^0,1)$ and $(1,1^1,0)$ levels. The horizontal error bars represent the range of matrix shifts due to multiple trapping sites. They were all excited on the strongest ν_3 line. In Xe this is site 2, in Kr it is site 1, and in Ar there is only one band. Solid points are $HC^{15}N$ in: Ar, matrix 30 excited at 3305.0 cm^{-1}, $k = (1.6 \pm 0.1) \times 10^6\ s^{-1}$; Kr, matrix 34 excited at 3287.0 cm^{-1}, $k = (5.9 \pm 0.3) \times 10^5\ s^{-1}$; Xe, matrix 32 excited at 3274.9 cm^{-1}. Unfilled points are $HC^{14}N$ in: Ar, matrix 14 excited at 3306.4 cm^{-1}, $k = (1.6 \pm 0.1) \times 10^6\ s^{-1}$; Xe, matrix 11 excited at 3276.2 cm^{-1}.

IV. ANALYSIS AND DISCUSSION OF RESULTS

A. Multiple sites

Fluorescence from the two ν_3 bands shows different decay rates at $M/A = 19\,060$ (Fig. 2). The diffusion of ν_3 quanta, discussed in the next section, shows that for $M/A = 19\,060$ an excitation of HCN in site 1 hops an average of 0.7 times to site 2 before relaxing and for site 2 there are 0.5 hops to site 1. This calculation agrees with the observation that the excitation is not fully equilibrated on the time scale of ν_3 relaxation. Because of hopping between these sites the measured rates are weighted averages of those for the truly isolated molecules.

The higher energy ν_3 band relaxes more slowly. This band has been assigned to site 1, the site which preserves the ν_2 degeneracy and is the more stable site (it increases in population with annealing). Since the ν_3 bands are red shifted in matrices, the vibrational frequency in this site is the least perturbed from the gas phase frequency. Both the splitting of the ν_2 degeneracy and the increased matrix shift indicate that there is more guest–host interaction in the site which decays more rapidly.

The change in rate with the vibrational frequency in the trapping site may be compared to the change with matrix shift in Fig. 9. The ends of the horizontal error bars on the unfilled square point show the transition frequencies for these two sites. The rates which fit the decays in Fig. 2(a) and 2(b) are 6.0×10^5 and $6.4 \times 10^5\ s^{-1}$, respectively. These produce a slope which is smaller in magnitude and opposite in direction compared to that drawn on Fig. 9. The intermolecular forces responsible for frequency shifts from matrix-to-matrix are not simply related to those which cause site splittings.

Fluorescence from the lower levels shows no dependence on excitation frequency. This could be because the difference in rate is within the noise, because energy diffuses among the sites on the time scale at which the lower levels relax, or because the excited molecule randomizes its orientation between the sites upon ν_3 relaxation as a result of local heating of the cage.

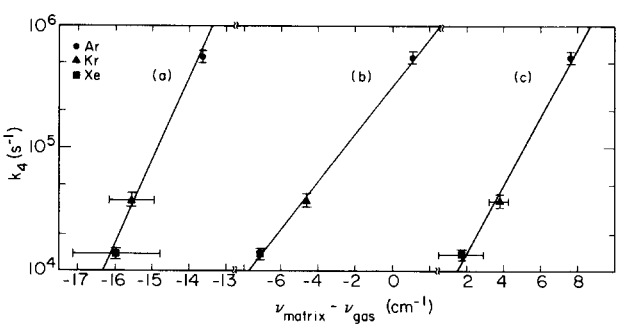

FIG. 10. Rate of ν_1 decay, observed via $(1,0^0,0)$–$(0,1^1,0)$, for $HC^{15}N$ in different hosts correlated with the matrix shift in the frequency of (a) the $(1,0^0,0) \rightarrow (0,2^0,0)$ nonradiative transition, (b) the $(1,0^0,0)$ level, and (c) the sum of the $(1,0^0,0)$ and $(0,2^0,0)$ levels. The same matrices and excitation frequencies were used as in Fig. 9. In Ar $k = (5.6 \pm 0.6) \times 10^5\ s^{-1}$ and in Kr $k = (3.7 \pm 0.4) \times 10^4\ s^{-1}$.

B. Energy diffusion

Energy can diffuse among guest species by dipole–dipole coupling. This has been modeled by Förster and others.[12–16] It has been analyzed for vibrational energy transfer in rare gas matrices by Legay[18] and by Wiesenfeld.[19] The energy may hop among like guest species or it may be transferred to a different species such as a dimer or an impurity molecule, which acts as an energy sink. To establish that the kinetics of a truly isolated molecule are being studied, the concentrations at which diffusion and quenching become significant must be determined.

The rate of transfer from a donor to an acceptor is[18]

$$C_{DA} = \frac{3}{512\pi^6 c n^4 \nu^6 R_{DA}^6} \frac{1}{\tau_D} \frac{1}{\tau_A} \int f_D(\nu) f_A(\nu)\, d\nu , \quad (1)$$

where R_{DA} is the distance between donor and acceptor, n is the refractive index, ν is the transition frequency, τ_D and τ_A are the donor and acceptor radiative lifetimes in the gas phase, and f_D and f_A are the line shape functions. For Lorentzian line shapes the overlap integral is[19]

$$\int f_D(\nu) f_A(\nu)\, d\nu = \frac{1}{2\pi} \frac{(\Delta\nu_A + \Delta\nu_D)}{(\nu_0^A - \nu_0^D)^2 + (\Delta\nu_A + \Delta\nu_D)^2/4} , \quad (2)$$

where ν_0 and $\Delta\nu$ are the line center and FWHM. When the transfer rate is summed over separation distances for donors and acceptors which are randomly distributed in a face centered cubic lattice, the rate is[18] $14.45\, x_A\, C_{DA}/d_0^6$ where x_A is the mole fraction of acceptors and d_0 is the lattice spacing between nearest neighbors (guests or host). For the diffusion of an excitation among identical molecules (donors) the average number of hops in time t is

$$N = \frac{14.45\, x_D\, C_{DD}}{d_0^6}\, t . \quad (3)$$

Two extreme cases of diffusion can be considered easily: (a) negligible diffusion among donor molecules on the time scale of vibrational relaxation and (b) rapid diffusion among donors. In the first case only transfer directly to a quenching site is considered. Excited molecules which are near such an acceptor relax rapidly compared to those which are isolated. The resulting decay of donor population is nonexponen-

tial[18]:

$$N_D(t) = N_D(0)\exp\left[-k_0 t - \frac{4\pi}{3} \times \Gamma(1-3/n)\, x_A\, \rho (C_{DA} t)^{3/n} \right]. \quad (4)$$

The unimolecular relaxation rate is k_0, Γ is the gamma function, x_A is the mole fraction of acceptors, ρ is the number density of lattice sites, and $n = 6$ for dipole–dipole interactions. If diffusion among donors is rapid, case (b), then all excitations are equivalent. When the transfer rate is summed over the donor to acceptor distances, the donor population becomes[18]

$$N_D(t) = N_D(0)\exp\left[-k_0 t - \frac{14.45\, x_A\, C_{DA}}{d_0^6} t \right]. \quad (5)$$

In the intermediate case those molecules which are near an acceptor relax rapidly as in case (a). On a longer time scale energy diffuses among donor sites until it decays unimolecularly or is quenched by transfer to an acceptor. This gives a nonexponential decay.

According to Eq. (1) diffusion is most important among levels with large integrated absorption intensities since $\nu^2 I_{\rm abs} \propto 1/\tau_{\rm rad}$. The line strengths of ν_2 and ν_3, determined from the spectrum, are approximately equal but ν_1 is 100 times weaker. Thus ν_2 and ν_3 quanta are expected to diffuse more rapidly. A modest change in rate from $(6.3 \pm 0.3)\times 10^5$ s^{-1} at $M/A = 19\,060$ to $(7.4 \pm 1)\times 10^5$ s^{-1} at $M/A = 900$ is observed for $(0,0^0,1)$ (Fig. 2). The $(0,1^1,0)$ fluorescence could not be entirely separated from that of other levels and so its concentration dependence could not be determined. The (1,0¶,0) fluorescence showed no concentration dependence. Interestingly, a weakly absorbing level, $(1,1^1,0)$, has the largest increase in rate with concentration, from $(1.3 \pm 0.2)\times 10^5$ s^{-1} at $M/A = 19\,060$ to $(2.9 \pm 0.6)\times 10^5$ s^{-1} at $M/A = 900$. This must be due to transfer of one quantum of ν_2 via

$$(1,1^1,0) + (0,0^0,0) \rightleftarrows (1,0^0,0) + (0,1^1,0) - 3\ \text{cm}^{-1}. \quad (6)$$

With this mechanism each nearly resonant hop relaxes the initial state, whereas $(0,0^0,1)$ is only relaxed unimolecularly or by hopping to a quenching site.

1. $(0,0^0,1)$

The average number of hops for a ν_3 quantum in HCN/Xe can be estimated with Eq. (3). The radiative lifetime of ν_3 is 13.5 ms in the gas phase.[20] The frequencies and linewidths of the ν_3 lines are $\nu = 3280.0$ cm^{-1}, $\Delta\nu = 2.0$ cm^{-1} and $\nu = 3276.2$ cm^{-1}, $\Delta\nu = 1.5$ cm^{-1} for sites 1 and 2, respectively. The relative populations are 42% in site 1 and 58% in site 2. The fluorescence decay time, 1.6 μs, was used for t. For a Xe matrix $n = 1.43$ and $d_0 = 4.34\times 10^{-8}$ cm.[18] For $M/A = 900$ the average number of hops is 61 for site 1 molecules and 96 for site 2. This includes contributions for hops both among one type of site and between the two types of sites. The hopping rate suggests that ν_3 relaxation occurs under conditions approaching the rapid diffusion limit, Eq. (5).

If the Einstein A value for the non-H-bonded C–H stretch in the dimer is assumed to be equal to that of the monomer, then the mole fraction of dimer can be obtained from the integrated absorbances in the spectrum. For $M/A = 19\,060$ no dimer is detectable so the decay rate is taken to be the unimolecular rate, k_0. For $M/A = 900$ there is 12% as much non-H-bonded dimer absorption, at 3267.8 cm^{-1} ($\Delta\nu = 1.5$ cm^{-1}), as total monomer absorption. Since dimer formation eliminates two monomers, the mole fraction of dimers is $x_A = 0.12/(1.24\times 900)$. Using these values, Eq. (5) gives the relaxation rate as 8.2×10^5 s^{-1} for site 1 and 9.6×10^5 s^{-1} for site 2 compared to 6.3×10^5 s^{-1} for k_0. Figure 2 shows that the decay becomes less exponential with increasing concentration as expected for this hopping mechanism since one site, site 2, is more nearly resonant with the quenching dimer. The measured rate at $M/A = 900$ is $(7.4 \pm 1)\times 10^5$ s^{-1} where the rate range corresponds to fitting the faster and slower parts of the nonexponential decay. Thus the hopping calculations in the limit of rapid diffusion overestimate the increase in rate with concentration.

There are a number of approximations in the theory and data which may be responsible. Legay's treatment is for near-resonant hops; hopping to the dimer is nonresonant by 8–12 cm^{-1}. A more rigorous development by Blumen, Lin, and Manz[13] treats phonon-assisted intramolecular transfer. While the choice of the rapid diffusion limit for ~ 100 hops per lifetime makes the problem tractable, it may not be correct. Random walk models[16] indicate that the dispersive diffusion limit may not be attained even after 10 000 hops. Additionally, though the line shapes were treated as Lorentzian, the ν_3 spectra can be best fit with a mixture of 20% Gaussian and 80% Lorentzian shapes.[4] Finally, nearest neighbor interactions have been treated equivalently to more distant ones even though many or all must actually be dimers.[19] These approximations would each give a calculated hopping rate which exceeds the true rate. There is also uncertainty in the concentrations of both monomer and dimer due to the assumptions that the matrix concentration equals that of the gas phase and that the ν_3 oscillator strength is unchanged by dimerization. Nonetheless, this calculation demonstrates that the magnitude of the increase in ν_3 decay rate and its nonexponentiality with concentration is consistent with excitation hopping among guest molecules and ultimately to a dimer.

The resonant hopping of ν_3 forces consideration of $(0,0^0,1) + (0,0^0,1) \rightleftarrows (0,0^0,2) + (0,0^0,0) + 110$ cm^{-1}. This is sufficiently nonresonant to require the absorption or emission of three lattice phonons for energy conservation. Blumen *et al.*[13] calculate that the macroscopic rate of this phonon assisted process is $\sqrt{10^{-5}}$ times that of the resonant hop. The probability of this hop is additionally reduced because only guest molecules excited to $(0,0^0,1)$ are acceptors (estimated below to be $\sim 8\%$). These two factors reduce the probability of a hop to $2\nu_3$ to $< 1\%$ at $M/A = 5000$.

2. $(1,1^1,0)$

Before calculating the hopping of a ν_2 quantum via Eq. (6), the many analogous hops must be considered: $(0,1^1,0) + (x,y,z) \rightleftarrows (0,0^0,0) + (x, y+1, z)$. For example, $(0,2^0,0)$ could be populated by a ν_2 quantum hopping to a

$(0,1^1,0)$ molecule. The relative probabilities of these processes may be determined by comparing the overlap integrals in Eqs. (1) and (2). Since every process other than Eq. (6) involves exciting ν_2 overtones, they are nonresonant by factors of χ_{22} and g_{22}. C_{DA} for Eq. (6) is an order of magnitude greater than for any of the analogous hops. Of course, both the forward and reverse processes in Eq. (6) must be considered. The forward and reverse rate constants differ by a Boltzmann factor.

For the nearly resonant dipole–dipole transfer of a bending quantum, Eq. (6), every ground state HCN is an acceptor molecule. The $(1,1^1,0)$ excitation cannot diffuse rapidly because the combination band has a weak absorbance so the negligible diffusion limit should apply. Since this is not a phonon-assisted process and since diffusion of $(1,1^1,0)$ is negligible, two of the approximations required in the treatment of ν_3 hopping are eliminated. Both $(0,1^1,0)$ and $(1,1^1,0)$ have three bands in the absorption spectrum (see Ref. 4) and so nine overlap integrals were evaluated using the following spectral data. The frequencies for the $\Delta v_2 = -1$ transitions from $(0,1^1,0)$ and $(1,1^1,0)$ are respectively 716.7 and 713.9 cm^{-1} in site 1, 718.4 and 715.5 cm^{-1} in site 2a, and 719.8 and 717.0 cm^{-1} in site 2b. The linewidths are 1.0 cm^{-1} in site 1 and 1.2 cm^{-1} in site 2. The best overlap is between site 2b $(1,1^1,0)$ and site 1 $(0,1^1,0)$, which are nonresonant by only 0.3 cm^{-1}. Based on the ν_3 radiative lifetime and the relative line strength of ν_2,[21] the gas phase ν_2 radiative lifetime is 540 ms. This lifetime was used to get C_{DA} from each of the nine overlap integrals.

The hopping rates from one donor site to both acceptor sites can be combined, but the time-dependent populations for each donor site must be treated separately. For $(1,1^1,0)$ hopping the above spectral data give for Eq. (4):

$$N_{110}(t) = 0.42\exp[-k_0 t - 7.7\times10^5 t^{1/2}/(M/A)] + 0.58\exp[-k_0 t - 2.4\times10^6 t^{1/2}/(M/A)] .$$

For the reverse process the rapid diffusion limit rather than the nondiffusion limit is preferred since each molecule in $(0,1^1,0)$ has $\sim5\times10^3$ hops per lifetime. From Eq. (3) the number of molecules which go back to $(1,1^1,0)$ in time interval Δt is

$$N_{010}(t)N_{100}(t)[0.42(1.2\times10^{11}) + 0.58(1.2\times10^{12})]\,\Delta t/(M/A)^2 .$$

There is a built-in bias in this treatment of the forward process of Eq. (6) as nondiffusive and the reverse as diffusive. Every $(1,1^1,0)$ molecule which is produced by hopping must have a ground state HCN acceptor nearby and will thus decay more rapidly than estimated for the nondiffusive limit. In practice this is not a serious problem for $M/A > 5000$ since $< 1\%$ of the molecules follow the reverse process in Eq. (6).

The time-dependent populations of $(1,1^1,0)$, $(1,0^0,0)$, and $(0,1^1,0)$ were calculated numerically by an iterative process. Initially the population entering $(1,1^1,0)$ from ν_3 relaxation was calculated in 0.5 μs intervals using the observed ν_3 decay. The increments of added population decay according to Eq. (4) and these contributions to the $(1,1^1,0)$ population were summed. For the time dependent ν_1 and ν_2 populations, the number hopping in from $(1,1^1,0)$ were added to populations obtained from unimolecular decay. Using these $(1,0^0,0)$ and $(0,1^1,0)$ populations the number of molecules which hop up to $(1,1^1,0)$ in each 0.5 μs time increment was calculated. Subsequent iterations included this hopping contribution as well as the ν_3 decay as sources of $(1,1^1,0)$ population inputs.

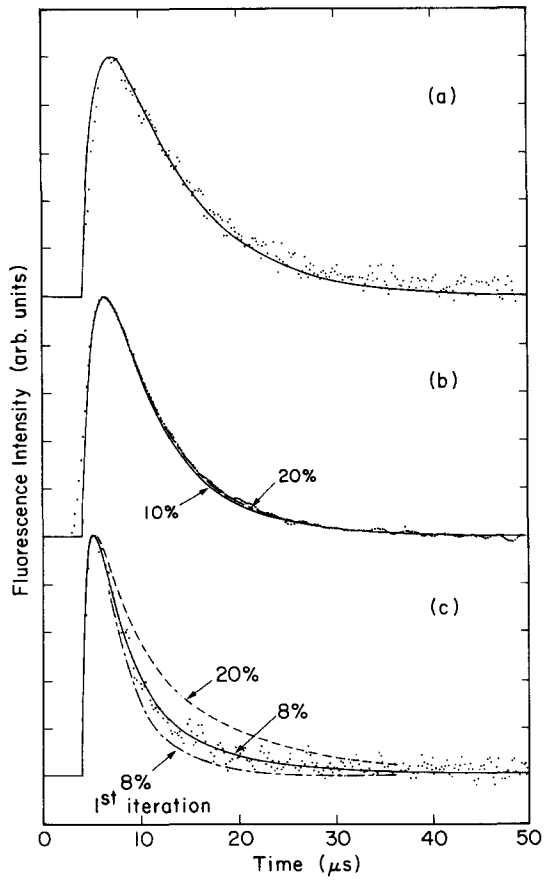

FIG. 11. Fluorescence from HCN/Xe $(1,1^1,0)$–$(0,0^0,0)$ as a function of concentration with calculated time dependent populations including Förster transfer. (a) Matrix 17, $M/A = 19\,060$, fit with the unimolecular decay rate, $\lambda_2 = k_0 = 1.3\times10^5\ s^{-1}$. (b) Matrix 11, $M/A = 5560$ with nearly identical calculated curves for 10% and 20% excitation. (c) Matrix 18, $M/A = 900$ with calculated curves for 8% and 20% excitation, the lower 8% curve neglects the repopulation of $(1,1^1,0)$ by hopping of a ν_2 quantum onto a $(1,0^0,0)$ molecule.

Figure 11 shows the $(1,1^1,0)$ fluorescence at three concentrations graphed with the calculated time dependent populations. At $M/A = 19\,060$ the effect of hopping is negligible and the data is fit with the unimolecular decay rate. At $M/A = 5560$ the $(1,1^1,0)$ decay rate is observably increased by hopping. In order to calculate the effect of hopping back to $(1,1^1,0)$, for which the acceptor is an excited molecule, the fraction of molecules which are excited by the laser must be known. Based on the ν_3 absorption cross section[21] and linewidth, and the beam energy and diameter, approximately 17% of the HCN molecules at the front surface of the matrix are excited. This fraction decreased through the thickness of the matrix with beam attenuation. The nearly identical theoretical curves for 10% and 20% excitation indicate that at this concentration only the forward process in Eq. (6) is important. Also the first iteration, which neglects

the reverse hopping, is nearly identical to subsequent iterations.

At $M/A = 900$ the change in the theoretical curve with the assumed fraction of molecules excited shows the importance of the reverse hop. Excellent agreement with the data is obtained for an average excitation of 8%. The first iteration of the solution includes only the forward part of Eq. (6) and decays faster than the data. When the iterations converge, the theoretical decay is slower because of the reverse part of Eq. (6). With 20% excitation the converged theoretical curve has too large a contribution from the reverse hop. At this concentration the bias against the forward hop discussed above could become important and would make the calculated decay too slow. With an exact treatment of the equilibrium in Eq. (6) the best agreement of theory and experiment would be for a $\gtrsim 8\%$ level of excitation.

Förster's model agrees excellently with this observation of resonant dipole–dipole energy transfer. The approximations of the theory should be reiterated. The spectral line shapes are not truly Lorentzian as assumed. The level of excitation varies with penetration depth and has been treated as an average excitation. Dimer formation upon sample deposition causes a departure from a random spatial distribution of HCN monomers by eliminating some or all HCN nearest neighbors. For concentrated samples both the forward and reverse processes in Eq. (6) are important and thus the acceptor molecules are no longer randomly distributed; at longer time scales $(1,1^1,0)$ with a nearby HCN neighbor is preferentially populated. A thorough set of experiments requires thin samples for uniform excitation, and measurements as a detailed function of laser fluence, temperature, and concentration. The main purpose of the present treatment is simply to understand the extent of intermolecular energy transfer so that the unimolecular relaxation may be analyzed correctly.

C. Kinetic scheme for intramolecular relaxation

The main features of the HCN/Xe relaxation behavior in dilute matrices are illustrated in Figs. 2–8. Unlike the relaxation of DCN/Xe, the decays of the ν_2 levels do not appear to follow the harmonic oscillator relation $k_{v,v-1} = vk_{1,0}$. The $(0,1^1,0)$, $(0,2^0,0)$, and $(1,0^0,0)$ levels have similar decay rates. There is a modest increase in rate with temperature for $(0,0^0,1)$ and a large increase for $(1,0^0,0)$. The emission spectra show that the population resides primarily in the ν_1 manifold at 9 K and in the ν_2 manifold at higher temperatures.

There is a mechanism which explains these observations and which is consistent with the DCN/Xe results. Since $(1,0^0,0)$ and $(0,3^1,0)$, and similarly $(1,1^1,0)$ and $(0,4^0,0)$, are in near resonance, the populations of these sets of levels should rapidly equilibrate via k_a, k_b, k_c, and k_d, shown in Fig. 1. The energy gap between $(1,1^1,0)$ and $(0,4^0,0)$ for HCN/Xe in site 1 is $\Delta E_{110\text{–}040} = 13\ \text{cm}^{-1}$. The gap between $(1,0^0,0)$ and $(0,3^1,0)$ is $\Delta E_{100\text{–}030} = 35\ \text{cm}^{-1}$. The levels in each pair have different symmetries so there is no Fermi resonance. These rates are related by

$$\frac{k_c}{k_d} = \sum_l g_l e^{-\Delta E_{10^00\text{–}03^10}/kT}. \tag{7}$$

Since $\Delta E_{100\text{–}030}$ is more than 5 times kT at 9 K, the equilibrium between $(0,3^1,0)$ and $(1,0^0,0)$ puts most of the excited molecules in the ν_1 state. If k_4 were small, the $(1,0^0,0)$ level would be an energy trap. If $k_4 \ll k_6$, k_7, the fluorescence decay from $2\nu_2$ and ν_2 would be governed by the rate at which population trickles into these levels, k_4. Thus fluorescence from the ν_1, ν_2, and $2\nu_2$ levels would all have similar decay times, as in Fig. 4. Since the $2\nu_2$ fluorescence decay would be limited by k_4 rather than k_6, its slow decay relative to $4\nu_2$ (Fig. 4) would not contradict the expectation that k_3 and k_6 are related by the factor of 2 for a harmonic oscillator. The large temperature dependence for ν_1 would be due to the increase in k_c/k_d with temperature. This would give an exponentially increasing rate of decay from ν_1 through the ν_2 manifold via $3\nu_2$. The increase in k_a and k_c with temperature would be responsible for the shift in population to the upper ν_2 manifold as shown in the emission spectra (Fig. 7).

To test this hypothesis the experiments were repeated with $HC^{15}N$/Xe. The C–H stretch and bend are only shifted by a few wave numbers but the C–N stretch is lowered by 32 cm^{-1} so that $\Delta E_{110\text{–}040} = 41\ \text{cm}^{-1}$ and $\Delta E_{100\text{–}030} = 62\ \text{cm}^{-1}$. This would make $(1,0^0,0)$ a much deeper energy trap. At 9 K the ν_1 route should be favored more over the upper ν_2 levels than was the case for $HC^{14}N$ and higher temperatures should be required to shift the pathway. The emission spectra in Fig. 8 agree with these expectations. Since the transition frequencies are separated more in $HC^{15}N$/Xe and the upper ν_2 levels are not populated at 9 K, this system was chosen for a complete kinetic analysis.

D. Method of analysis

The kinetic scheme with 12 rate constants in Fig. 1 produces a set of seven simultaneous first-order linear differential equations, as in the case of DCN relaxation.[1] These differential equations were solved with matrix techniques to yield seven eigenvalues (decay rate constants) and seven time-dependent populations. Some of the eigenvalues correspond to single k_i's in Fig. 1 and some are functions (not necessarily simple sums) of several. Input k_i's were varied within the constraints of the model below until the solutions to these equations (output eigenvalues and amplitudes) fitted the observed fluorescence. Following the results of the DCN/Xe experiments,[1] the rate constants for the ν_2 manifold were assumed to be proportional to the ν_2 quantum number following the harmonic oscillator model[22]:

$$k_3/4 = k_5/3 = k_6/2 = k_7/1 = k_8/1\ . \tag{8}$$

Similarly, k_2 and k_4 each require $\Delta v_2 = 2$ and are proportional to $v_2(v_2 - 1)$:

$$k_2 = \frac{3(3-1)}{2(2-1)} k_4 = 3\,k_4\ . \tag{9}$$

The l levels were assumed to equilibrate rapidly with phonons at the matrix temperature as was found for the rotational levels of matrix isolated HCl.[23] The pairs of rates k_a, k_b and k_c, k_d are related by detailed balance as in Eq. (7). The exoer-

TABLE III. Rate constants for $HC^{15}N$/Xe and $HC^{14}N$/Xe relaxation at 9 K.

Transition	Rate constant (s^{-1}) $HC^{15}N$[a]	$HC^{14}N$[b]
$(0,0^0,0)\rightarrow(1,1^1,0)$	$k_1 = (4.7 \pm 0.3)\times 10^5$	$(6.3 \pm 0.3)\times 10^5$
$(1,1^1,0)\rightarrow(1,3^1,0)$	$k_2 = 4.08\times 10^4$	2.4×10^4
$(0,4^0,0)\rightarrow(0,3^1,0)$	$k_3 = 3.2\times 10^5$	4.0×10^5
$(1,0^0,0)\rightarrow(0,2^0,0)$	$k_4 = (1.36 \pm 0.1)\times 10^4$	$(8.0 \pm 1.0)\times 10^3$
$(0,3^1,0)\rightarrow(0,2^0,0)$	$k_5 = 2.4\times 10^5$	3.0×10^5
$(0,2^0,0)\rightarrow(0,1^1,0)$	$k_6 = (1.6 \pm 0.2)\times 10^5$	2.0×10^5
$(0,1^1,0)\rightarrow(0,0^0,0)$	$k_7 = 8.0\times 10^4$	$(1.0 \pm 0.2)\times 10^5$
$(1,1^1,0)\rightarrow(1,0^0,0)$[c]	$k_8 = (9.9 \pm 2)\times 10^4$	1.2×10^5
$(1,1^1,0)\rightarrow(0,4^0,0)$	$k_a = 7.8\times 10^5$	7.1×10^7
$(0,4^0,0)\rightarrow(1,1^1,0)$	$k_b = 1.0\times 10^9$	1×10^9
$(1,0^0,0)\rightarrow(0,3^1,0)$	$k_c = 9.9\times 10^4$	7.2×10^6
$(0,3^1,0)\rightarrow(1,0^0,0)$	$k_d = 1.0\times 10^9$	1×10^9

[a] Rate constants reported without error bars have not been measured directly; see the text for method of estimating error.
[b] The errors reported for k_4 and k_7 reflect the range of c_1 and c_2 (by which the $HC^{15}N$ rates are multiplied) which fit the data.
[c] These rates are for matrices with $M/A = 5000$–7000 and k_8 includes the effect of hopping via Eq. (6). Figure 3 shows that λ_2 is $\sim 16\%$ larger than at infinite dilution for $HC^{14}N$; k_8 at infinite dilution is $(9.5 \pm 2)\times 10^4\ s^{-1}$ for $HC^{14}N$ and $(7.7 \pm 2)\times 10^4\ s^{-1}$ for $HC^{15}N$.

gic rate constants k_b and k_d were chosen to be much greater than any other rate. An increase from 10^9 to $10^{11}\ s^{-1}$ had no effect on the results. The temperature dependence of the numerically subscripted rate constants was taken from a model in which the vibrational energy is transferred to guest modes and one phonon is emitted to conserve energy, as was found to be the case for the ν_2 levels of DCN/Xe.[1] Varying the lettered rate constants in the same way had no effect on the fit; it depends only on the ratios k_a/k_b and k_c/k_d.

E. Rates for $HC^{15}N$/Xe relaxation at 9 K

Tables III and IV show the rates and time dependent populations which are the solutions to the coupled rate equations which best fit the data at 9 K. The initial amplitude of the pumped state, $(0,0^0,1)$ is 1. The peak amplitude of lower states is always less than 1. Although some of the coefficients of the exponential decays in Table IV are larger than 1, these are balanced by negative amplitudes for terms with similar rate constants. The maximum population for each level is listed. This is not the fraction of the molecules which decay through each level, it is the maximum fraction which are in the level at any one time.

1. $(0,0^0,1)$

Fluorescence decays from $(0,0^0,1)$ are similar to those for $HC^{14}N$, Fig. 2. They cannot be described with a single decay rate. The "error" margins in Table III correspond to fitting the faster and slower portions of the decay.

2. $(1,1^1,0)$

The $(1,1^1,0)$ level was monitored by the $(1,1^1,0)$–$(1,0^0,0)$ transition. This could not be completely filtered from $(0,1^1,0)$–$(0,0^0,0)$, $(0,2^0,0)$–$(0,1^1,0)$, and $(0,2^2,0)$–$(0,1^1,0)$. In order to compare the fit to the data, the calculated time dependent populations for these four levels were weighted and summed. For the CVF position at which the fluorescence was recorded, the transmittance of each transition was determined from calibration curves, as presented in Ref. 1. The amplitude of fluorescence from each level is proportional to the Einstein A value of the transition. For a harmonic oscillator these follow the same relations as the rate constants in Eqs. (8) and (9). For transitions which originate in an upper l level, the amplitude depends on the thermal population of that level. Based on a Boltzmann distribution, the $l = 2$ states will have 3.5% as much population as $l = 0$ at 9 K and the $l = 3$ and 4 states will be negligibly populated. Thus while the fluorescence from $(0,2^2,0)$ cannot be eliminated by the CVF, its intensity is weighted by its small population. For $(0,1^1,0)$ fluorescence, which is partially self-absorbed, the observed fluorescence intensity is the emitted intensity times the fraction which is transmitted by the matrix. For front surface excitation, the percent transmission calculated from the spectrum of $HC^{15}N$/Xe, matrix 32, is 77%.

The net effect is shown in Fig. 12(a). The fluorescence is fit with the time dependent populations from Table IV weighted for CVF transmission, Einstein A, l population, and self-absorption: $(1,1^1,0) + 0.33\ (0,2^0,0) + 0.07\ (0,1^1,0)$. Since the l levels were assumed to equilibrate rapidly the

TABLE IV. Time dependent populations of $HC^{15}N$/Xe levels at 9 K.[a,b]

Level	Eigenvalue, λ (s^{-1}) 4.7×10^5	1.4×10^5	1.0×10^9	1.36×10^4	1.0×1.0^9	1.6×10^5	8.0×10^4	Max N[c]
(001)	1	0	0	0	0	0	0	1
(110)	−1.45	1.45	0	0	0	0	0	0.590
(040)	-1.7×10^{-3}	1.7×10^{-3}	~	0	0	0	0	6.4×10^{-4}
(100)	0.47	−1.61	~	1.14	0	0	0	0.773
(030)	-4.4×10^{-5}	7.1×10^{-6}	~	3.7×10^{-5}	~	0	0	3.5×10^{-5}
(020)	−0.02	−1.11	~	0.11	~	1.02	0	0.062
(010)	0.01	2.94	~	0.26	~	−2.04	−1.16	0.111

[a] The population of each level is the sum of the amplitudes times the exponential of the eigenvalue at the top of the column: $\Sigma a_i e^{-\lambda_i t}$. For example, $N(110) = -1.45\exp(-4.7\times 10^5\ t) + 1.45\exp(-1.4\times 10^5\ t)$.
[b] ~ is used for amplitudes which are approximately, but not exactly, zero.
[c] System starts with $N_0 = 1$ in $(0,0^0,1)$.

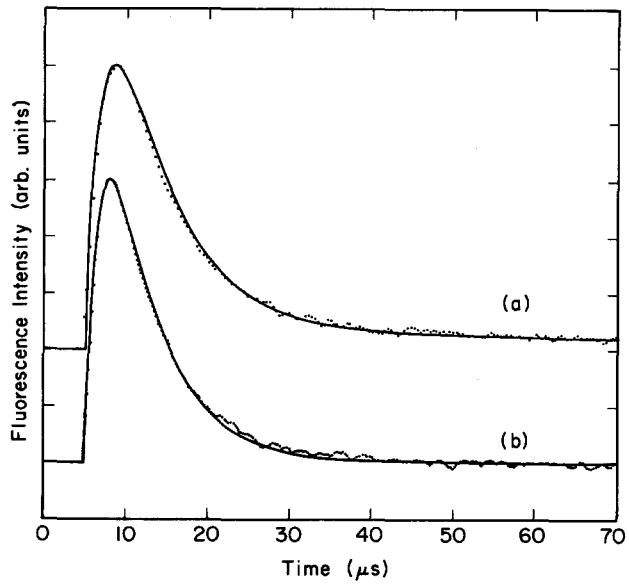

FIG. 12. (a) Fluorescence for $HC^{15}N/Xe$, matrix 32, $M/A = 7210$, 9 K, with the CVF centered at 709 cm^{-1}. The fit is $(1,1^1,0) + 0.33(0,2^0,0) + 0.07(0,1^1,0)$ using the populations from Table IV. The signal has not returned to the base line because of the slow $(0,1^1,0)$ decay. (b) $(1,1^1,0)$–$(0,0^0,0)$ fluorescence from $HC^{14}N/Xe$ at 9 K, fit with the $(1,1^1,0)$ population from Table V. The data is from matrix 11, $M/A = 5560$. There are no other transitions which interfere at this frequency.

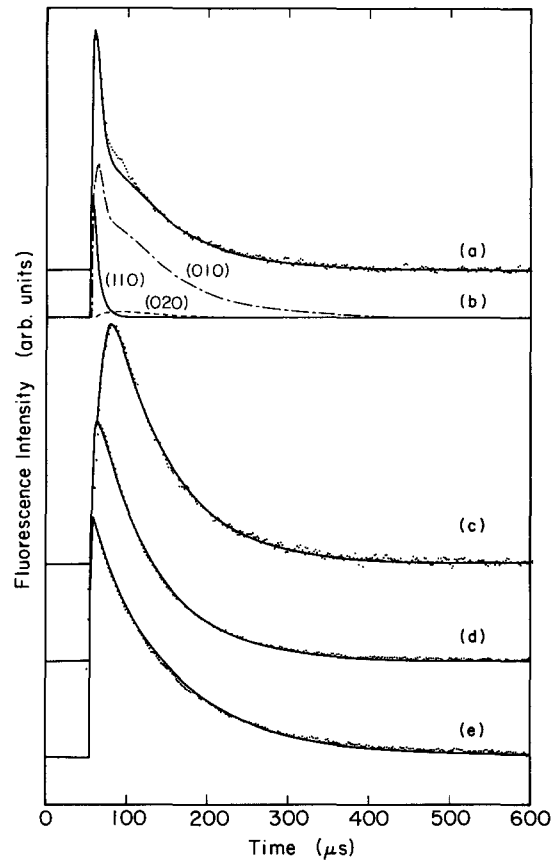

FIG. 13. Fluorescence from $HC^{15}N/Xe$, matrix 32, $M/A = 7210$, 9 K. (a) CVF centered at 720 cm^{-1}. The fit is $(0,1^1,0) + 0.27(0,2^0,0) + 0.23(1,1^1,0)$. The fast decay is $(1,1^1,0)$ and the hopping contribution to $(0,1^1,0)$. The slow decay is dominated by k_4. (b) The individual components of the above fit. (c) $(0,2^0,0)$–$(0.0^0,0)$ fluorescence at 1416 cm^{-1}. The fit is the $(0,2^0,0)$ population from Table IV. The decay is dominated by k_4. (d) Fluorescence from difference frequency transitions $(1,0^0,0)$–$(0,1^1,0)$ and $(1,1^1,0)$–$(0,2^1,0)$ with the CVF centered at 1340 cm^{-1}. The fit is equally weighted $(1,1^1,0)$ and $(1,0^0,0)$ from Table IV. (e) Fluorescence from the same transition as (c) but from $HC^{14}N/Xe$ at 9 K, fit with populations from Table V: $1.35(1,1^1,0) + (1,0^0,0)$. The data is from matrix 22, $M/A = 5690$, with the CVF at 1380 cm^{-1}.

$(0,2^0,0)$ and $(0,2^2,0)$ contributions, 0.27 and 0.06 respectively, have been summed. Since the decays of $(0,2^0,0)$ and $(0,1^1,0)$ are governed by the slow rate, k_4, they are more than an order of magnitude slower than the $(1,1^1,0)$ decay. Thus the fit of the fast decay in Fig. 12 is sensitive to the $(1,1^1,0)$ decay rate, $\lambda_2 = k_2 + k_8$, and is unaffected by changes in $(0,2^0,0)$ and $(0,1^1,0)$. To extract k_8 from this sum, the rate constant k_2 was determined from k_4 (see below). Only k_8 was varied to fit the data in Fig. 12. The k_8 uncertainty in Table III was set by the rate constants for which the data and fit no longer overlap. This value of k_8 includes an exponential approximation to the 25% contribution from hopping discussed in the next section.

3. k_4

The fluorescence decays of levels below $(1,0^0,0)$, i.e., $(0,2^0,0)$ and $(0,1^1,0)$, are governed by the slow decay of $(1,0^0,0)$, k_4. Since $(1,0^0,0)$–$(0,0^0,0)$ cannot be filtered from $(1,1^1,0)$–$(0,1^1,0)$, the best transition with which to measure k_4 is $(0,2^0,0)$–$(0,0^0,0)$. The emission spectrum in Fig. 8 shows that $(0,3^1,0)$ and $(0,4^0,0)$ are not populated at 9 K so the CVF could select exclusively $(0,2^0,0)$ fluorescence. Figure 13(c) shows the $(0,2^0,0)$ fluorescence fit with the $(0,2^0,0)$ population from Table IV. Since k_4 is the slowest rate, this fit is primarily sensitive to changes in k_4. The reported k_4 error comes from the rate constants for which the data and fit in Fig. 13(c) do not overlap. Since k_2 cannot be measured independently, it was determined from k_4 via Eq. (9) and no error bars are reported.

While $(1,0^0,0)$ fluorescence also decays with k_4, it is less useful in determining k_4 because it could not be separated from $(1,1^1,0)$. Figure 13(d) shows fluorescence with equal contributions from both levels plotted with the populations from Table IV. No parameters were varied for this fit. The plot verifies that the $(1,1^1,0)$ and $(1,0^0,0)$ rate constants, determined from fluorescence from other levels, also fit this data.

Similarly, the slowest decay rate for $(0,1^1,0)$ is k_4. The hopping mechanism in Eq. (6) populates $(0,1^1,0)$ before the initially excited molecules relax to this level. The $(0,1^1,0)$ population produced by hopping decay with k_7 rather than with k_4. This contribution to the $(0,1^1,0)$ fluorescence both rises and falls more rapidly than that produced by the unimolecular decay. The time dependent $(0,1^1,0)$ and $(1,0^0,0)$ populations including the hopping contribution were calculated as part of the iterative solution to the $(1,1^1,0)$ population. Figure 13(b) shows the calculated $(0,1^1,0)$ population with the hopping contribution evident. At this concentration, $M/A = 7210$, 25% of the molecules hop from $(1,1^1,0)$ and 75% decay unimolecularly. Only 0.7% do the reverse hop. The $(1,0^0,0)$ population is not greatly affected by including hopping because the rate at which hopping populates

$(1,0^0,0)$ is comparable to the unimolecular rate.

The fit of the $\Delta v_2 = 1$ fluorescence in Fig. 13(a) includes the time dependent populations: $(0,1^1,0) + 0.27$ $(0,2^0,0) + 0.23$ $(1,1^1,0)$. The $(0,2^2,0)$–$(0,1^1,0)$ transition is transmitted at this frequency; however, the $(0,2^2,0)$ kinetics are assumed to be the same as the $(0,2^0,0)$. The individual contributions to the fluorescence are shown in Fig. 13(b). The rate constants were determined by fits to other data. No parameters were varied for this fit.

4. (0,n,0)

The upper ν_2 levels are not populated at 9 K and the decay of the lower ones is governed by the $(1,0^0,0)$ decay, k_4, so the only data which directly yields the ν_2 manifold kinetics is the $(0,2^0,0)$ rise. All of the rate constants except k_6 have been fixed by the decays of $(0,0^0,1)$, $(1,1^1,0)$, and $(0,2^0,0)$. Table IV shows that k_6 is the same order of magnitude as the rise terms (those with negative amplitudes) in $(0,2^0,0)$. When k_6 is varied, it has no effect on the slow fall of $(0,2^0,0)$. Figure 14 shows the change in the fit of the $(0,2^0,0)$ rise with a change in k_6. This graph demonstrates that the rise is in fact sensitive to k_6. These two fits are used for the k_6 error bars. The other ν_2 rates are set according to the harmonic oscillator relation, $k_{v,v-1} = vk_{1,0}$. This model successfully fit the ν_2 levels of DCN/Xe. There is no way to test it in HCN/Xe since only k_6 can be independently determined from the data. However, the harmonic oscillator model predicts that $k_8 = k_7 = k_6/2$. While k_7 could not be observed, the rates in Table III show that, except for the contribution from hopping via Eq. (6), k_8 is equal to $k_6/2$, thus supporting this model.

F. Temperature dependence

1. (0,0^0,1)

The temperature dependence of the $(0,0^0,1)$ decay, k_1, is shown in Fig. 5. The solid lines show the temperature dependence expected if the vibrational energy is transferred to a local guest motion and one phonon is excited to conserve energy.[1,17,19] A 25 cm^{-1} phonon fits the observed temperature dependence.

2. (1,0^0,0)

The $(1,0^0,0)$ level has the largest temperature dependence (Fig. 6). The lower solid line is the temperature dependence which is predicted by the model of the $(1,0^0,0)$ level of $HC^{15}N$ relaxing via $(0,2^0,0)$ at 9 K and also via $(0,3^1,0)$ and $(0,3^3,0)$ at higher temperatures. Since there are two $3\nu_2$ levels, each of which is doubly degenerate, the expression given by detailed balance is (site 1)

$$\frac{N_{(0,3^1,0)} + N_{(0,3^3,0)}}{N_{(1,0^0,0)}} = \frac{k_c}{k_d} = 2\,e^{-62/kT} + 2e^{-101/kT}, \qquad (10)$$

where the energy gaps from $(1,0^0,0)$ to $(0,3^1,0)$ and $(0,3^3,0)$ are 62 and 101 cm^{-1}, respectively. The analogous equation for $(1,1^1,0)$ and the $4\nu_2$ levels gives $k_a/k_b = (1/2)\exp(-41/kT) + (2/2)\exp(-60/kT) + (2/2)\exp(-120/kT)$. Equation (10) provides the temperature dependence for k_c; k_d was held constant. For the fit of the $HC^{15}N$ data in Fig. 6, k_4 and k_2 depend on exciting a 20 cm^{-1} phonon and $k_{3,5,6,7,\text{ and }8}$ depend on exciting a 15 cm^{-1} phonon. The temperature dependence of the k_1 rate constant was measured directly (Fig. 5). If k_4 were assigned a larger temperature dependence, then the calculated decay rates would increase too fast at low temperatures; if k_5 had a smaller temperature dependence, then the calculated rates would increase too slowly at high temperatures. Thus by varying only the phonon sizes for the k_4 and k_5 decay to local modes within a reasonable range, this model fits the temperature dependence of the $(1,0^0,0)$ decay well.

G. Rates for $HC^{14}N$/Xe

The emission spectrum of $HC^{14}N$/Xe in Fig. 7 shows that even at 9 K some of the population relaxes via $4\nu_2$ and $3\nu_2$. This makes it difficult to determine a set of rate constants. Whereas in $HC^{15}N$/Xe the $(1,0^0,0)$ decay gave k_4 directly, for $HC^{14}N$/Xe there is also a contribution from k_5 via k_c. Similarly the $(1,1^1,0)$ decay rate has, in addition to $k_2 + k_8$, a contribution from k_3 via k_a. The rate constants of the ν_2 manifold were obtained from the rise of the $(0,2^0,0)$ fluorescence of $HC^{15}N$/Xe. In $HC^{14}N$/Xe the $(0,2^0,0)$ kinetics are more complicated because it is populated through two channels instead of one. However, since a set of rate constants has been determined for $HC^{15}N$/Xe, it should be possible to make some small changes to fit the $HC^{14}N$/Xe data.

The only rate constant which can be independently determined is k_1 for the $(0,0^0,1)$ decay. The decay rate is faster for the ^{14}N isotope. This may result from the 32 cm^{-1} smaller energy gap between $(0,0^0,1)$ and $(1,1^1,0)$ for $HC^{14}N$/Xe. The same energy gap argument predicts that k_4, the rate constant for $(1,0^0,0) \rightarrow (0,2^0,0)$, should be smaller for $HC^{14}N$/Xe since this energy gap is 30 cm^{-1} larger. The ν_2 relaxation rates should be relatively unchanged since the C–H bending frequency is shifted by only 1 cm^{-1}.

The $HC^{14}N$/Xe data was fit as follows. The $(0,0^0,1)$ decay gave k_1 directly. The rate constants k_2 and k_4 were assumed to differ from the $HC^{15}N$/Xe values by a multiple, c_1. The $\Delta v_2 = -1$ rate constants were multiplied by c_2. These

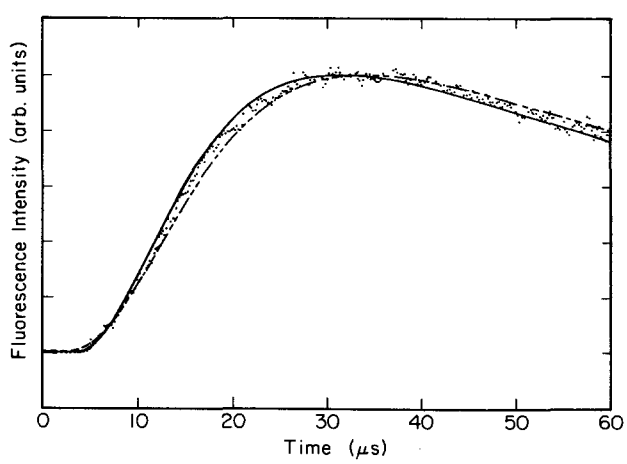

FIG. 14. Rise of $(0,2^0,0)$ fluorescence at 1416 cm^{-1} from $HC^{15}N$/Xe with the two fits which represent the upper and lower limits to the rate k_6 shown in Table III. Data from matrix 32, $M/A = 7210$ at 9 K.

TABLE V. Time dependent populations of $HC^{14}N$/Xe levels at 9 K.[a]

Level	Eigenvalue, λ (s^{-1})							Max N
	6.3×10^{5}	1.6×10^{5}	1.1×10^{-9}	9.9×10^{3}	1.0×10^{9}	2.0×10^{5}	1.0×10^{5}	
(001)	1	0	0	0	0	0	0	1
(110)	−1.26	1.26	0	0	0	0	0	0.589
(040)	−0.081	0.081	~	0	0	0	0	0.038
(100)	0.34	−1.42	~	1.08	0	0	0	0.825
(030)	2.1×10^{-3}	-9.1×10^{-3}	~	7.0×10^{-3}	~	0	0	5.4×10^{-3}
(020)	−0.01	−0.35	~	0.06	~	0.30	0	0.040
(010)	~	1.17	~	0.13	~	−0.60	−0.70	0.073

[a] Same footnotes as Table IV.

two variable parameters were determined from the fluorescence from two levels: $(1,1^1,0)$ and $(1,0^0,0)$. Each of these levels depends on both c_1 and c_2. Table III lists the rates which fit the $HC^{14}N$/Xe fluorescence best. They differ from the ^{15}N rates by $c_1 = 0.59 \pm 0.07$ and $c_2 = 1.25 \mp 0.25$. The time dependent populations are listed in Table V. The fits to the $(1,1^1,0)$ and $(1,0^0,0)$ fluorescence are shown in Figs. 12(b) and 13(e). Fluorescence from the other levels is equally well fit.

The error quoted in Table III for k_1 comes from graphing rates which over- and underestimate the data. The other errors assume that the $HC^{15}N$/Xe rates are correct and that the uncertainty is in the correlated multipliers, c_1 and c_2. The errors listed for k_4 and k_7 represent the biggest change in each constant which permits both $(1,1^1,0)$ and $(1,0^0,0)$ to be fit by varying the other constant.

The maximum population of each level during the relaxation is listed in the Tables IV and V. The populations of $(0,4^0,0)$ and $(0,3^1,0)$ are two orders of magnitude larger for $HC^{14}N$. This is in pleasing agreement with the 9 K emission spectra (Figs. 7 and 8) in which fluorescence from $(0,4^0,0)$ was observed for $HC^{14}N$ but not for $HC^{15}N$. These populations also reproduce the curious minimum in fluorescence intensity at the frequency where $(0,3^1,0)$–$(0,1^1,0)$ fluorescence is expected for $HC^{14}N$ (Fig. 7). The maximum population of a level, and therefore the peak fluorescence intensity, depends on both the fraction of molecules which decay through the level and on the kinetics of the level. When the production rate is increased relative to the loss, the maximum population increases. Even though $(0,3^1,0)$ has more molecules relax through it than does $(0,4^0,0)$, the rise is slower so the maximum population is less. The emission spectrum shows more fluorescence from $(0,4^0,0)$ than $(0,2^0,0)$ while Table V lists a larger maximum population for $(0,2^0,0)$. This is because the fluorescence intensity is the product of the population and the Einstein A value, which is six times larger for the $(0,4^0,0)$ transition.

To test both this method of getting the $HC^{14}N$/Xe rates and the model of the temperature dependence, the fluorescence decay of $(1,0^0,0)$ at higher temperatures was calculated. The lettered rate constants were obtained by detailed balance as in Eq. (10) with energy gaps of 13, 34, and 97 cm^{-1} for k_a/k_b and of 35 and 77 cm^{-1} for k_c/k_d. The $(0,0^0,1)$ decay was observed directly. As with $HC^{15}N$/Xe the temperature dependence of k_2 and k_4 was assumed to depend on the emission of a single 20 cm^{-1} phonon. All the other rates were assumed to increase as for a 15 cm^{-1} phonon. Figure 6 shows $(1,0^0,0)$ temperature dependence data and the fit which was calculated without any adjustable parameters. Although this model slightly overestimates the rates, the temperature dependence is reproduced well. Increasing the phonon sizes by 5 cm^{-1} brings the fit into agreement with the data. The decay rate increases more with temperature for $HC^{14}N$ because the energy gap, $\Delta E_{100-030}$, is smaller.

H. Host effect

The large increase in relaxation rate as the matrix host is changed from Xe to Kr to Ar is correlated to the matrix shift in Figs. 9 and 10. The shift in vibrational frequency from the gas phase to the matrix environment is a measure of the intermolecular forces between the guest and host. The long range attractive forces are due to (1) the interaction of the permanent charge distributions between the molecules, (2) the interaction between the permanent dipole of the guest and the induced charge distribution of the rare gas, and (3) the interaction between the instantaneous charge distributions. At short distances the overlap of the valence electrons causes a repulsive interaction.

Previous studies of vibrational relaxation in matrices[2,23–25] have shown that for the loss of a single vibrational quantum there is a correlation between the matrix shift in the transition frequency with various hosts and the decay rate. In particular, the rate seems to be exponentially correlated to some interaction parameter with which the matrix shift is linearly correlated.

The relaxation of HCN involves complicated transitions in which several quanta are changed. Figures 9 and 10 show that for k_1, $(0,0^0,1)\rightarrow(1,1^1,0)$, and k_4, $(1,0^0,0)\rightarrow(0,2^0,0)$, there are equally good correlations between the rate and (a) the matrix shift in the transition frequency, (b) the matrix shift in the upper state frequency, and (c) the sum of the matrix shifts of the upper and lower state frequencies. Abouaf-Marguin and Gauthier-Roy[25] found that for CH_3F and CD_3F the slopes of these lines are greater when the relaxation rates are smaller. The slopes for k_1 of $HC^{15}N$ and k_4 of $HC^{14}N$ and $HC^{15}N$ follow the same trend of increased slope with decreased relaxation rate. Since the rates increase as the vibrational frequencies increase from matrix to matrix, the repulsive interaction is most likely responsible for

the relaxation kinetics. Recent work[23] for HCl in rare gas matrices is in striking contrast. As the vibrational frequency increases, the rate decreases ($k_{Xe} > k_{Kr} > k_{Ar}$). Thus the attractive potential appears to be responsible for the relaxation of HCl; the matrix shift is still correlated to the decay rate but with the opposite sign.

V. A BINARY COLLISION MODEL FOR VIBRATIONAL ENERGY TRANSFER IN MATRICES

The relaxation rates for all three isotopic hydrogen cyanides in Xe are determined by the same interaction potential. This offers a unique opportunity for testing theoretical models against the observed effects of quantum number change, vibrational energy change, and isotopic substitution. The modest temperature dependence of vibrational relaxation rates of matrix isolated molecules shows that energy is initially transferred to local modes of the guest rather than directly to bulk phonons of the matrix.[18,19,22,23] Thus relaxation processes involve interactions between the molecule and the nearest neighbor atoms of the matrix cage. For several systems vibrational relaxation rates in condensed phases have been found to correspond to gas phase relaxation rates scaled up by the increase in binary collision rate.[26] Thus relaxation seems likely to occur primarily as the result of binary collisions between the excited molecule and the matrix cage. The increase in relaxation rate, $k_{Xe} < k_{Kr} < k_{Ar}$, with steepness of the repulsive intermolecular potential is seen for gas phase vibrational energy transfers caused by hard, repulsive, binary encounters. The translational motion of the vibrationally excited molecule with respect to the matrix cage is dominated by phonon zero-point motion. It is possible, therefore, to transfer theories for vibrational relaxation in gas phase collisions to the matrix situation. Should this approach be viable, the extensive knowledge of gas phase processes will permit predictions of relaxation mechanisms and relative rates for matrix isolated systems.

A. Gas phase theory

A variety of first-order perturbation treatments have been developed for treating vibrational relaxation in gas phase collisions.[5,22,27–30] Most are successful in reproducing the essential features of observations. The theory developed by Schwartz, Slawsky, and Herzfeld (SSH)[5] and extended to polyatomics by Tanczos[27] gives the probability that a binary collision will induce a change in vibrational quantum state by transferring vibrational energy to translational energy. The intermolecular potential is assumed to be $V_r = V_0 \exp(-\alpha r)$, where r is the distance between the atoms which collide. The probability per collision for $V \rightarrow V$ transfer in first order is[5]

$$P^{0-F} = V^2 \frac{1}{16\pi^2} g_F (\theta_0^2 - \theta_F^2)^2 \frac{(e^{\theta_0} - e^{-\theta_0})(e^{\theta_F} - e^{-\theta_F})}{(e^{\theta_0} + e^{-\theta_0} - e^{\theta_F} - e^{-\theta_F})^2}, \tag{11}$$

where $\theta_0 = 4\pi^2 \mu \nu_0 / \alpha h$, g_F is the degeneracy of the final state, and μ is the reduced mass of the collision pair. The initial and final relative velocities are related by

$$\tfrac{1}{2}\mu(v_F^2 - v_0^2) = \Delta E, \tag{12}$$

where ΔE is the energy lost from vibration.

The vibrational factor, V, is the matrix element of the powers of the normal coordinate which appear in the expansion of the intermolecular potential. The net vibrational factor is a product of the factors for each vibration whose quantum number changes. For 0,1,2,3, and 4 quantum jumps these matrix elements are

$$V_{i,i}^2 = 1, \tag{13a}$$

$$V_{i,i+1}^2 = \frac{\alpha^2(\overline{A^2})}{2\gamma}(i+1), \tag{13b}$$

$$V_{i,i+2}^2 = \left(\frac{1}{2!}\right)^2 \left[\frac{\alpha^2(\overline{A^2})}{2\gamma}\right]^2 (i+1)(i+2), \tag{13c}$$

$$V_{i,i+3}^2 = \left(\frac{1}{3!}\right)^2 \left[\frac{\alpha^2(\overline{A^2})}{2\gamma}\right]^3 (i+1)(i+2)(i+3), \tag{13d}$$

$$V_{i,i+4}^2 = \left(\frac{1}{4!}\right)^2 \left[\frac{\alpha^2(\overline{A^2})}{2\gamma}\right]^4 (i+1)(i+2)(i+3)(i+4), \tag{13e}$$

where

$$\gamma = \frac{4\pi^2 \nu}{h}, \tag{14}$$

and $V_{i,j} = V_{j,i}$. The vibrational factors are dimensionless quantities. The repulsive intermolecular force constant α is in units of reciprocal length. $\overline{A^2}$, the averaged sum of the Cartesian displacements for a unit change in the normal coordinate (assumed to contribute fully to r), is in units of reciprocal mass. Equations (13a)–(13c) are adapted from Stretton.[28]

B. Adaptation to matrices

This theory may be adapted to "collisions" of HCN with the Xe cage to calculate the rates of vibrational transitions. For a matrix isolated molecule the collision velocities are well defined. The initial velocity is due to the phonon zero point energy and the final velocity is obtained via Eq. (12). If the entire matrix is considered to be the collision partner, $\mu = m_{HCN}$. This is approximately true even for a collision with a single Xe atom. The potential parameter α is unknown; gas phase values for similar molecules are about 5 $Å^{-1}$.[22,30] For a diatomic molecule the amplitude of vibration of the colliding atom is[30]

$$(\overline{A^2}) = \frac{m_y}{m_x(m_x + m_y)} + \frac{m_x}{m_y(m_x + m_y)}. \tag{15}$$

The modes of HCN were treated as for a pseudodiatomic molecule with X = H for the C–H stretch and bend and X = N for the C–N stretch. The amplitude of the C–H bend obtained from the G matrix is slightly greater than that for the stretch; the latter was chosen to approximate the fraction of motion of the bending H atom toward the matrix. The values used for $\overline{A^2}$ are listed in the footnotes to Table VI.

Table VI lists the vibrational factors for the isotopes of HCN for $\alpha = 6$ $Å^{-1}$. For sets of transitions such as (0,v,0)→(0,v − 1,0), v = 1, 2, 3, and 4 only one rate is shown since the others were fixed in the ratios given by the harmonic oscillator matrix elements.

TABLE VI. SSH parameters for V→T and V→R in HCN/Xe.

	Transition	k (s^{-1})	ΔE[a] (cm^{-1})	Δn	V^2 (V→T)[b,c]	$\theta_F - \theta_0$[d] V→T	$\theta_F - \theta_0$[d] V→R
$HC^{14}N$	(001)→(110)	6.3×10^5	476.6	3	3.12×10^{-3}	18.6	8.7
	(100)→(020)	8.0×10^3	671.6	3	1.81×10^{-3}	23.5	11.7
	(010)→(000)	1.0×10^5	716.7	1	0.815	24.6	12.3
$HC^{15}N$	(001)→(110)	4.7×10^5	508.4	3	3.10×10^{-3}	19.8	9.1
	(100)→(020)	1.4×10^4	641.2	3	1.81×10^{-3}	23.2	11.1
	(010)→(000)	8.0×10^4	715.7	1	0.818	25.0	12.2
DCN	(001)→(110)	3×10^8	120.5	3	1.20×10^{-3}	6.5	3.1
	(100)→(030)	8.8×10^6	213.4	4	1.73×10^{-5}	10.4	5.3
	(040)→(100)	1×10^4[e]	341.6	5	2.32×10^{-7}	14.9	8.2
	(010)→(000)	2.1×10^5	573.2	1	0.494	21.5	12.8

[a] Site 1 frequencies.
[b] These V^2 values are for $\alpha = 6$ Å^{-1} as for V→T. Since $V^2 \propto \alpha^{2\Delta n}$, the values for V→R, with $\alpha = 3$ Å^{-1}, differ from these by factors of appropriate powers of 0.5.
[c] The following values of A^2 (in amu^{-1}) were used for the C–N stretch and bend, and for the C–N stretch: $HC^{14}N$, 0.964 and 0.074; $HC^{15}N$, 0.966 and 0.072; DCN, 0.467 and 0.071.
[d] The vibrational energy is transferred to either translation or rotation. These θ's were calculated with an initial translational or librational energy of 100 cm^{-1}. For V→T, $\alpha = 6$ Å^{-1} and for V→R, $\alpha = 3$ Å^{-1}.
[e] This rate corresponds to the harmonic oscillator case with $n = 1$ in Eq. (4), Ref. 1.

The terms in Eq. (11) which involve θ_0 and θ_F can be simplified based on their relative magnitudes. An initial translation energy of 100 cm^{-1} and $\alpha = 6$ Å^{-1} give $\theta_0 = 13.2$. For a transition with $\Delta E = 476.6$ cm^{-1}, Eq. (12) gives $\theta_F = 31.8$. Thus $e^{\theta_0} \gg e^{-\theta_0}$, $e^{\theta_F} \gg e^{-\theta_F}$, and $e^{\theta_0} - e^{\theta_F} \simeq -e^{\theta_F}$. Equation (11) may then be rearranged to give a "normalized" relaxation rate:

$$k_N \equiv \frac{16\pi^2}{V^2(\theta_0^2 - \theta_F^2)^2 g_F} k = \Gamma e^{(\theta_0 - \theta_F)}. \quad (16)$$

The relaxation rate k has been substituted for the collision probability via $k = \Gamma P$ where Γ is the collision rate. The term $(\theta_0^2 - \theta_F^2)^2$ is proportional to $\mu \Delta E^2$.

C. Results of SSH calculations

1. V→T

The rates of the transitions in Table VI are plotted as a function of energy gap in Fig. 15. While there is a general trend of decreasing rate with increasing energy gap, the rates for DCN transitions with $\Delta n = 4$ and 5 are slower than the

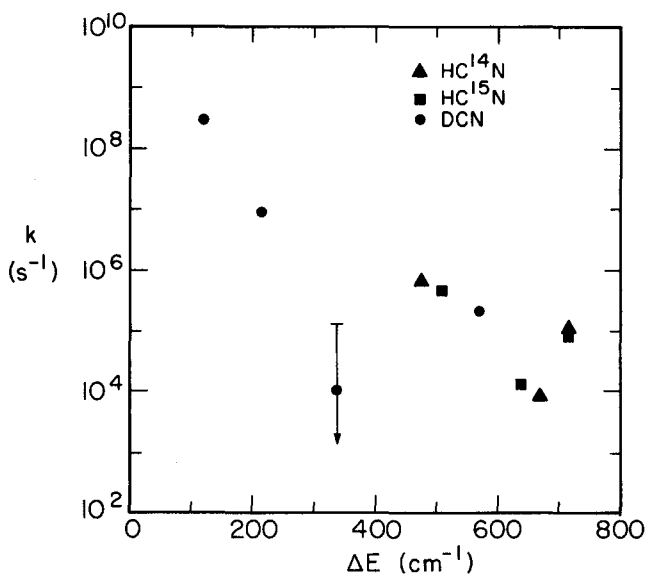

FIG. 15. Decay rates for vibrational transitions of HCN isotopes plotted as a function of energy gap. Table VI lists the transitions represented by each point. For most of the points the error bars are small on this vertical scale; for (0,4^0,0) → (1,0^0,0) for DCN only an upper limit is known. The rates do not decrease monotonically as the energy gap increases.

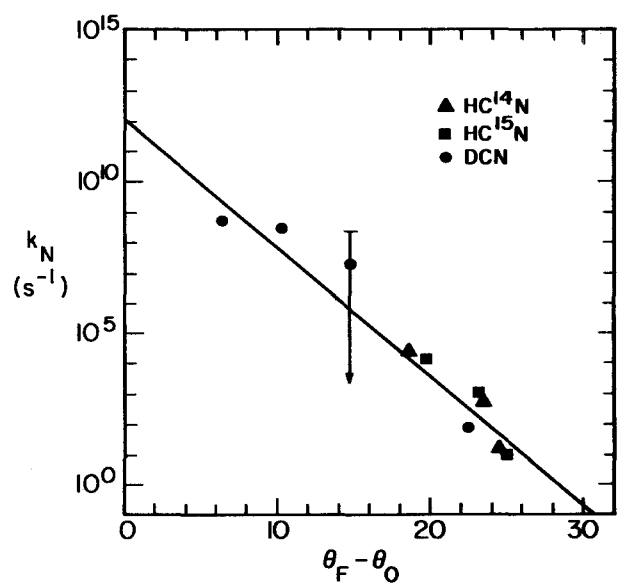

FIG. 16. Correlation of rate constants to ΔE and Δn via SSH theory for V → T transfer. The y axis is normalized rate constant, Eq. (16). The solid line has slope −0.43, as required by theory, and intercept 1.3×10^{12} s^{-1}.

trend indicates and the HCN transitions with $\Delta n = 1$ are faster.

Normalizing the rate constants as in Eq. (16) is an attempt to quantitatively incorporate the effect of the quantum number change along with the effect of the energy gap. According to Eq. (16), a logarithmic plot of k_N vs $\theta_0 - \theta_F$ should produce a straight line with slope $-\log_{10}e = -0.43$, and intercept Γ. Figure 16 shows this plot for $\alpha = 6$ Å^{-1} and $E_0 = 100$ cm^{-1}. A least-squares fit of these points gives slope -0.43 and intercept 1.3×10^{12} s^{-1}. The slope is in perfect agreement with Eq. (16) and the intercept is a reasonable collision frequency for a molecule trapped in a Xe matrix. The normalized DCN rates with $\Delta n = 4$ and 5 fall slightly above the line. This indicates that the vibrational factors in Eqs. (13d) and (13e) overestimate the decrease in rate with increasing Δn. Since only an upper limit is rigorously known for k_9 in DCN,[1] this point is indicated with a long downward arrow and was not included in the least-squares fits.

The values of α, E_0, and A^2 may be varied within reasonable ranges. Reasonable values of α are within the range 5 ± 2 Å^{-1}. Both V^2 and θ are dependent on α. All of the normalized rate constants have the same dependence on θ but $V^2 \propto \alpha^{2\Delta n}$ so a decrease in α produces a relative increase in k_N for transitions with large Δn. This plot is not a sensitive measure of α, but for $\alpha = 6$ Å^{-1} the scatter in the data is less than for smaller values of α because k_N for the DCN points with $\Delta n = 4$ and 5 increase with decreasing α. The value of α varies with matrix host. The ν_1 and ν_3 decays fit on this plot if $\alpha = 6.5$ Å^{-1} in Kr and 7 Å^{-1} in Ar.

The initial translational energy, E_0, is related to the local phonon frequency[17] (about 70 cm^{-1} for a light to medium mass guest[31]). E_0 may be chosen between the phonon zero point energy in one direction, 35 cm^{-1}, and the total energy for three directions of translation and two of libration. The normalized rate is independent of E_0 but both θ_F and θ_0 are affected. The entire plot is translated to the left for larger and to the right for smaller E_0. In addition, varying E_0 has a greater effect on small θ_F, for which E_0 is a larger fraction of the total E_F. Thus, for smaller E_0 the absolute value of the slope is decreased and the intercept is increased. For example, $E_0 = 35$ cm^{-1} gives slope -0.41 and intercept 2.1×10^{13} s^{-1}. These are also in reasonable agreement with Eq. (16), so the conclusions are not dependent on the value of E_0 selected.

Finally, the amplitude coefficient A^2 is less than the values in Table VI if only part of the vibrational motion is directed toward a matrix atom. If A^2 is smaller for the C–H bend than for the stretches, then k_N is increased for transitions involving Δv_2. As in the case of decreased α, this serves primarily to increase the normalized rates for DCN transitions with $\Delta n = 4$ and 5.

The graph in Fig. 16 may be used to check the consistency of the choice of $k_{a,b,c,d}$ used to solve for the relaxation rate constants. These lettered rate constants, which determine the rate of approach to thermal equilibrium between the near-resonant energy levels, were chosen arbitrarily. They were constrained to be much larger than the other rate constants and to have the ratios k_a/k_b and k_c/k_d required by detailed balancing. Only k_d may be normalized via Eq. (16) since k_b does not satisfy $e^{\theta_0} - e^{\theta_F} \approx e^{-\theta_F}$ and both k_a and k_c are endothermic. For k_d, $\theta_F - \theta_0 = 3.68$, and the line on Fig. 16 yields $k_d = 2.0\times10^8$ s^{-1}, less than the 10^9 s^{-1} value assumed, but still much too large to influence the observed kinetics.

2. V→R

The work of Legay, Bondybey, Brus, and others has shown that vibrational excitation in matrices can be transferred to rotation.[18,19,32] V→R and V→T,R transfer has been investigated in much detail for gas phase systems.[22,29,30,33] When the mass associated with rotation is much smaller than for translation (e.g., a hydride rotation in which heavy atoms are all very near the axis of rotation), rotation is the preferred accepting mode. This results from the better match of rotational velocity with vibrational frequencies. The collision theory may be handled approximately by substituting rotational velocities for translational ones.[33] The librational velocity is used for v_0 and the rotational velocity for v_F.[17] If the vibrational energy is transferred to rotational energy, then

$$\Delta E = \frac{1}{2} I\omega^2 = \frac{1}{2}\frac{Iv_R^2}{d^2}, \tag{17}$$

where I is the moment of inertia, d is the distance from the H atom to the center of mass and $v_F^2 = v_0^2 + v_R^2$. While μ, used in V→T calculations, is almost unchanged by isotopic substitution, I is 22% larger for DCN than for HCN. The repulsive force constant, α, of about 3 Å^{-1} fits most gas phase data on V→R transfers.[33]

Figure 17 shows the normalized rate constants for the V→R model. The shift of the DCN points to the right compared to the V→T plot is due to the larger moment of inertia

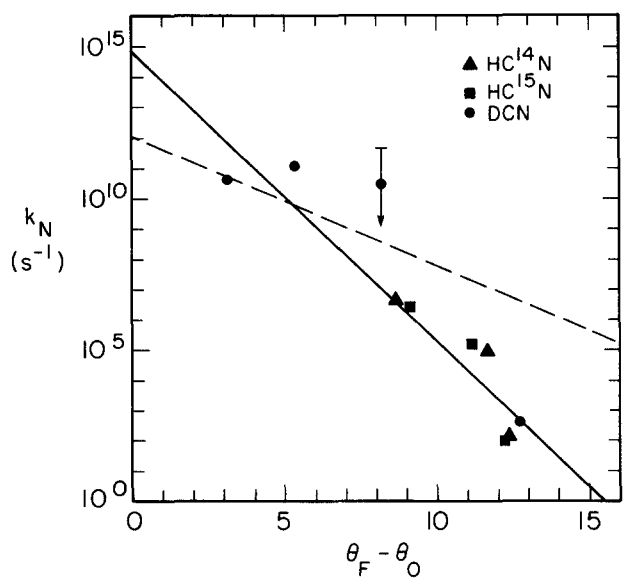

FIG. 17. Correlation of rate constants to ΔE and Δn via SSH theory for V → R transfer. The solid line is a least-squares fit to the data with slope -1.05 and intercept 6.5×10^{14} s^{-1}. The broken line shows the slope and approximate intercept for the theory.

of DCN. The large normalized rates for the DCN transitions with $\Delta n = 4$ and 5 are due to the small value of α. The solid line is a least-squares fit of the data, again excluding the $\Delta n = 5$ point, with slope -1.05 and intercept 6.5×10^{14} s^{-1}. The broken line shows the fit predicted by Eq. (16). No variation of α, E_0, and A^2 makes the data approach the theory. This strongly suggests that V→R transfer is not the dominant relaxation mechanism.

Further evidence that rotation is not the primary accepting mode comes from a comparison of the rate constants for the single quantum transition $(0,1^1,0) \rightarrow (0,0^0,0)$ to those predicted by Legay's correlation. In his Fig. 6 in Ref. 18, he shows a linear correlation between log k and J_m, the minimum number of rotational quanta required to match the vibrational energy. This correlation is successful for a large number of diatomic and polyatomic molecules. For both HCN and DCN $J_m = 22$ and Legay's correlation predicts $k = 10^2$ s^{-1}. That the measured rate constants are three orders of magnitude larger suggests that V→R is not important.

VI. CONCLUSIONS

Matrix isolated HCN provides a remarkable system in which to test models of vibrational relaxation in the solid state. These experiments provide complete sets of rate constants for single and multiple quantum transitions of three isotopes of HCN in Xe. In addition, the relaxation was studied as a function of trapping site, temperature, concentration, and matrix host.

The relaxation of DCN down the ν_2 vibrational ladder follows the prediction for a harmonic oscillator: $k_{v,v-1} = v \times k_{1,0}$. The modest increase in rate with temperature indicates that the energy is transferred to a local guest mode with only one lattice phonon required to match the energies.

In HCN the near resonance of $(1,0^0,0)$ with $(0,3^1,0)$, and of $(1,1^1,0)$ with $(0,4^0,0)$ creates an energy trap in $(1,0^0,0)$. At 9 K the thermal equilibrium channels most of the population into $(1,0^0,0)$, from which only a small fraction can escape via $(0,3^1,0)$. With increased temperature the primary relaxation route changes from the ν_1 to the ν_2 manifold. A large, metastable population inversion exists between $(1,0^0,0)$ and both $(0,2^0,0)$ and $(0,1^1,0)$ during most of the relaxation. Laser action on these transitions would certainly be possible. Such a trapping mechanism has ramifications for attempts at tailoring laser-induced reactions. If the metastable state vibration were the reaction coordinate, increased quantum yields could be expected. If the thermally activated vibration were along the reaction coordinate, then an unusually high temperature dependence could result.

The relaxation rate and the matrix shift both increase in the order Xe < Kr < Ar. This indicates that the repulsive part of the guest–host interaction is primarily responsible for the relaxation. The spectra reveal two trapping sites for HCN/Xe, with HCN along either the ⟨111⟩ or ⟨110⟩ axis. The latter probably involves a H-bonding type interaction between HCN and Xe.[4] Independent excitation of the ν_3 absorption of these two sites produced measurably different ν_3 decay rates with a faster decay in the site with greater interaction.

Increasing the HCN concentration produces a modest increase in the $(0,0^0,1)$ decay and a large increase in the $(1,1^1,0)$ decay. Förster theory for dipole–dipole transfer successfully describes the hopping of vibrational quanta. The $(0,0^0,1)$ resonant hopping is rapid compared to relaxation. The increase in the $(1,1^1,0)$ decay rate with concentration is due to the hopping of a ν_2 quantum to a neighboring guest. For this case theory is tested quantitatively by the experiment.

Rate constants were measured for transitions involving from one to five vibrational quanta. Rates do not increase monotonically with energy gap. The SSH[5] theory for hard repulsive collisions is successfully adapted from the gas phase to describe changes in both vibrational quantum number and vibrational energy. The data are fit well for energy transfer to translation but not to rotation. Since the heavy atoms move in the rotation of HCN, its rotational velocities and quanta are small by contrast to those of hydrides for which rotation is known to be involved in vibrational relaxation in gases or matrices.

This success of gas phase binary collision theory in describing complex transitions in matrix isolated molecules raises the possibility of predicting relaxation rates and especially relative magnitudes of rates in new systems. Fitting the measured rates only required choosing reasonable values for the intermolecular force constant and the initial translational or librational energy. The difficulty in making predictions is determining whether the accepting mode is translation or rotation and whether repulsive or attractive forces cause the transfer. The situation could also be complicated by symmetry considerations. Bondybey and English observed rapid vibrational transfer between levels of NCO in Ar which were in Fermi resonance.[34] Based on quantum yields of C_2H_4 reactions in N_2 matrices, Frei and Pimentel proposed that nonradiative transitions between states with g and u symmetry are forbidden.[35] It must be pointed out that the SSH theory is quite approximate for gas phase collisions. This application in matrices is certainly crude and will be limited in its applicability. Nonetheless, it should now be possible to predict relative orders of magnitude of relaxation rate constants in many systems and therefore predict relaxation paths. This will be important in considering low temperature infrared photochemical reaction systems and in predicting systems such as HCN in which inverted population distributions may be produced and energy stored.

ACKNOWLEDGMENTS

We are grateful to the U. S. Army Research Office, Research Triangle Park, NC for support of this research. We are very much indebted to Linda Young who recorded preliminary absorption spectra and fluorescence decays. Henry Luftman provided the original program for solving rate equations. We thank Jay Wiesenfeld and Linda Young for extensive discussions of binary collision models and we thank Michael Fayer for discussions of intermolecular energy transfer.

[1] A. D. Abbate and C. B. Moore, J. Chem. Phys. **82**, 1263 (1985).
[2] L. Young and C. B. Moore, J. Chem. Phys. **76**, 5869 (1982).

[3]V. A. Apkarian and E. Weitz, Chem. Phys. Lett. **76**, 68 (1980).
[4]A. D. Abbate and C. B. Moore, J. Chem. Phys. **82**, 1255 (1985).
[5]R. N. Schwartz, Z. I. Slawsky, and K. F. Herzfeld, J. Chem. Phys. **20**, 1591 (1952).
[6]H. Dubost and R. Charneau, Chem. Phys. **12**, 407 (1976).
[7]L. Abouaf-Marguin, B. Gautheir-Roy, and F. Legay, Chem. Phys. **23**, 443 (1977).
[8]J. Goodman and L. E. Brus, J. Chem. Phys. **65**, 1156 (1976).
[9]L. J. Allamandola, H. M. Rojhantalab, J. W. Nibler, and T. Chappell, J. Chem. Phys. **67**, 99 (1977).
[10]D. R. Lutz, K. A. Nelson, C. R. Gochanour, and M. D. Fayer, Chem. Phys. **58**, 325 (1981).
[11]R. W. Tkach, T. R. Gosnell, and A. J. Sievers, Opt. Lett. **10**, 122 (1984).
[12]Th. Förster, Ann. Phys. **2**, 55 (1948); D. L. Dexter, J. Chem. Phys. **21**, 836 (1953).
[13]A. Blumen, S. H. Lin, and J. Manz, J. Chem. Phys. **69**, 881 (1978).
[14]J. Manz, Chem. Phys. **24**, 51 (1977).
[15]J. Manz, Chem. Phys. Lett. **51**, 477 (1977).
[16]R. F. Loring, H. C. Andersen, and M. D. Fayer, J. Chem. Phys. **76**, 2015 (1982); Chem. Phys. **85**, 149 (1984).
[17]J. M. Wiesenfeld, Thesis, University of California, Berkeley, 1977.
[18]F. Legay, in *Chemical and Biological Applications of Lasers*, edited by C. B. Moore (Academic, New York, 1977), Vol. II, Chap. 2.
[19]J. M. Wiesenfeld and C. B. Moore, J. Chem. Phys. **70**, 930 (1979).
[20]A. Hariri, A. B. Petersen, and C. Wittig, J. Chem. Phys. **65**, 1872 (1976).
[21]K. Kim and W. T. King, J. Chem. Phys. **71**, 1967 (1979).
[22]J. T. Yardley, *Introduction to Molecular Energy Transfer* (Academic, New York, 1980), pp. 82–170.
[23]L. Young and C. B. Moore, J. Chem. Phys. **81**, 3137 (1984).
[24]B. Gauthier-Roy, L. Abouaf-Marguin, and F. Legay, Chem. Phys. **46**, 31 (1980).
[25]L. Abouaf-Marguin and B. Gauthier-Roy, Chem. Phys. **51**, 213 (1980).
[26]M. Châtelet, J. Kieffer, and B. Oksengorn, Chem. Phys. **79**, 413 (1983), and references therein.
[27]F. I. Tanczos, J. Chem. Phys. **25**, 439 (1956).
[28]J. L. Stretton, Trans. Faraday Soc. **61**, 1053 (1965).
[29]J. T. Yardley and C. B. Moore, J. Chem. Phys. **49**, 1111 (1968).
[30]J. D. Lambert, *Vibrational and Rotational Relaxation in Gases* (Clarendon, Oxford, 1977), Chap. 3.
[31]M. Berkowitz and R. B. Gerber, Chem. Phys. **37**, 369).
[32]L. E. Brus and V. E. Bondybey, in *Radiationless Transitions*, edited by S. H. Lin (Academic, New York, 1980), Chap. 6.
[33]P. F. Zttel and C. B. Moore, J. Chem. Phys. **58**, 2004, 2922 (1973); Science **182**, 541 (1973).
[34]V. E. Bondybey and J. H. English, J. Chem. Phys. **67**, 2868 (1977).
[35]H. Frei and G. C. Pimentel, J. Chem. Phys. **78**, 3698 (1983).